TOPICAL REVIEW — Amorphous physics and materials

# Universal properties of relaxation and diffusion in condensed matter

K L Ngai(倪嘉陵)[1,2,†]

[1] CNR-IPCF, Dipartimento di Fisica, Università di Pisa, Largo B. Pontecorvo 3, I-56127, Pisa, Italy
[2] State Key Laboratory of Metastable Materials Science and Technology, Yanshan University, Qinhuangdao 066004, China

(Received 9 October 2016; published online 8 December 2016)

By and large the research communities today are not fully aware of the remarkable universality in the dynamic properties of many-body relaxation/diffusion processes manifested in experiments and simulations on condensed matter with diverse chemical compositions and physical structures. I shall demonstrate the universality first from the dynamic processes in glass-forming systems. This is reinforced by strikingly similar properties of different processes in contrasting interacting systems all having nothing to do with glass transition. The examples given here include glass-forming systems of diverse chemical compositions and physical structures, conductivity relaxation of ionic conductors (liquid, glassy, and crystalline), translation and orientation ordered phase of rigid molecule, and polymer chain dynamics. Universality is also found in the change of dynamics when dimension is reduced to nanometer size in widely different systems. The remarkable universality indicates that many-body relaxation/diffusion is governed by fundamental physics to be unveiled. One candidate is classical chaos on which the coupling model is based, Universal properties predicted by this model are in accord with diverse experiments and simulations.

**Keywords:** many-body relaxation/diffusion, universal dynamics, coupling model, classical chaos

**PACS:** 81.05.Kf, 81.05.Lg, 81.07.–b, 89.75.–k **DOI:** 10.1088/1674-1056/26/1/018105

## 1. Introduction

Condensed matters composed of molecules, atoms, or ions are densely packed with nontrivial interactions between these basic structural units. Naturally relaxation and diffusion of the units are controlled by the interaction, and are necessary a many-body problem. More than a century has passed since Einstein[1] solved the (one-body) Brownian diffusion problem,[2] and surprisingly has yet to appear is a full solution of the many-body problem with general acceptance. Perhaps this is not totally surprising because the interaction potentials are usually anharmonic, and the motion in phase space is governed by classical chaos,[3–5] which is hard to deal with theoretically, and that is even before relaxation and diffusion have to be dealt with as a problem of irreversible process in statistical mechanics. Notwithstanding, my very first paper on the subject published in 1979[1] did recognize the need to solve this many-body problem of irreversible processes before their dynamics can be understood, and made the first attempt based on semi-classical quantization of classical chaos,[6] and followed by other treatments of classical chaos.[7–11] These attempts summarily referred to these days as the coupling model (CM) yield predictions of the dynamic properties which are universal and should be applicable to relaxation and diffusion processes in various condensed matters. That was more than thirty years ago, when there was hardly any significant experimental evidence supporting the claim. Notwithstanding, motivated by this hunch I entered into different fields involving widely dissimilar systems to see if the predictions of the CM apply generally, and to find significant evidences for universality. The effort over the last three decades has paid off. Solid and significant experimental evidences gathered in diversely different systems[11] enable me to affirm that the dynamics of many-body relaxation and diffusion in interacting systems are universal. This assertion is important not only that it reveals a general manifestation from nature, but also it implies the existence of fundamental physics behind it.

I shall demonstrate the universality first from the dynamic processes in glass-forming systems. This is reinforced by strikingly similar properties of different processes in contrasting interacting systems all having nothing to do with glass transition. The examples given here for glassforming systems have diverse chemical compositions and physical structures, translation and orientation ordered phase of rigid molecule, and polymer including chain dynamics. For conductivity relaxation of ionic conductors, the universal properties are found in liquid, glassy, and crystalline materials with contrasting chemical and physical properties.[11,12] Readers who are working in the fields are already familiar with properties such as non-exponential time dependence of correlation function and the length-scale of the heterogeneous dynamics. These properties are generally found in many-body relaxation and diffusion of interacting systems, and are parallel consequences of the many-body nature of the relaxation. However, these properties alone are not deep enough as evidence for universality. The properties that I shall use to support universality are

†Corresponding author. E-mail: Kia.Ngai@pi.ipcf.cnr.it

© 2017 Chinese Physical Society and IOP Publishing Ltd 

more sophisticated, fundamental, and quantitative in nature, far beyond non-exponentiality, dynamic heterogeneity and its length-scale. A few examples are given in this review. More can be found in my books, one published 5 years ago[11] and the other one most recently.[12] The only element that the diverse systems considered have in common is anharmonic interaction between the elemental units, which makes the relaxation and diffusion a many-body process and the dynamics become universal.

The universal properties are in accord with either the predictions of the CM or its conceptual basis, and are introduced naturally in conjunction with the CM in the following sections. However, the main purpose of this review is to make the readers aware of the universality of the dynamic properties of many-body relaxation/diffusion processes in wide variety of condensed matters with diverse chemical compositions and physical structures. Therefore coverage of the theoretical basis and predictions of the CM is minimized here but details can be found in references.[7–11]

## 2. Glass-forming systems

Among interacting systems of present interest, glass-formers are most abundant and also widely studied in their many-body relaxation and diffusion properties by experiments and simulations. Glass-formers can be inorganic, organic, polymeric, ionic, biomolecular, metallic, colloidal, and even artificial such as the bead-necklace model for polymer or binary mixtures of large and small particles, both interacting with the Lennard–Jones potential. The immense diversity in chemical bonding, composition, and physical structure makes glass-formers the best testing ground to find evidence for universality if it exists at all.

Any property found can be identified with one of the universal properties associated with many-body relaxation/diffusion if any of its surrogate is related to or governing the property. The surrogate I have chosen is a measure of the deviation of the correlation function $\phi(t)$ from the exponential time dependence. One choice is the parameter $n$ in the exponent of the Kohlrausch stretched exponential function, $\phi(t) = \exp[-(t/\tau)^{1-n}]$, used to fit the correlation function. Alternatively the full-width at half-maximum of the susceptibility can be used since it is proportional to $n$. In all examples of universal properties to be given below and much more in the books,[11,12] $n$ is involved and instrumental. One of the basic predictions of the CM is the Kohlrausch (K) stretched exponential correlation function where $n$ is called the coupling parameter. The second basic prediction of the CM given by the relation[7–11]

$$\tau(T,P,\lambda,\ldots) = [(t_c)^{-n}\tau_0(T,P,\lambda,\ldots)]^{1/(1-n)}. \quad (1)$$

The equation shows explicitly that $n$ determines the observed many-body relaxation time $\tau$, and its dependence on temperature $T$ and pressure $P$, or any other variable $\lambda$ by raising to the power $1/(1-n)$.

The time $t_c$ in Eq. (1) is the onset time of chaos caused by the anharmonic interaction, and is also the crossover time of the correlation function from $\phi(t) = \exp(-t/\tau_0)$ for one-body relaxation to $\phi(t) = \exp[-(t/\tau)^{1-n}]$ for many-body relaxation. The magnitude of $t_c$ depends on the strength of interaction. The crossover was found in the structural relaxation of polymeric and small molecular glass-formers,[11] the conductivity relaxation of ionic conductors, the dynamics of entangled polymer chains in bulk or in semidilute solutions, unentangled polymer chains in highly asymmetric polymer blends, polymer cluster solutions, and glassy ionic conductors.[11,12] The crossover at $t_c$ is one of universal properties. The one-body relaxation time $\tau_0$ (the primitive relaxation time of the CM) is directly obtained from the dependence of the $\exp(-t/\tau)$ correlation function before it crosses over to $\phi(t) = \exp[-(t/\tau)^{1-n}]$ after $t_c$.

### 2.1. Indicator of many-body relaxation: $n$

Stronger interaction giving rise to larger $n$ in diverse systems is another universal property, which we elucidate by three examples. The first is a bead-necklace model of polymer, where the beads with diameter $\sigma$ fixed at 4.0 Å are separated at distance $l$ and interacting with Lennard–Jones potential. Inter-bead interaction is increased on decreasing $l$. This trend is reflected by the increase of $n$ in the K-function fit to the torsional autocorrelation function (TACF) obtained by simulations[13] in Fig. 1.

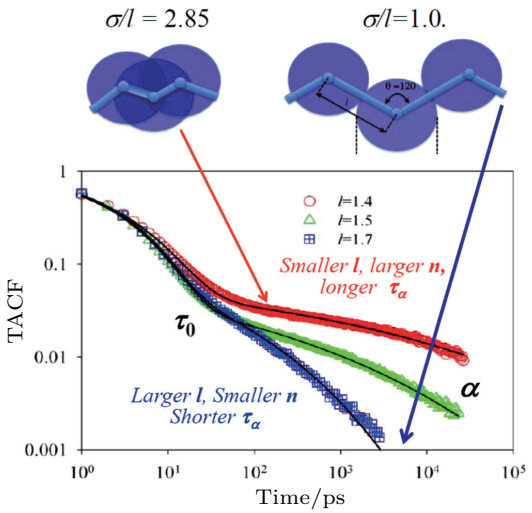



**Fig. 1.** (color online) TACF from simulations of bead-necklace model of polymer at 100 K for $l = 1.4$ Å, 1.5 Å, and 1.7 Å. Solid lines show fits to the JG $\beta$-relaxation and the $\alpha$-relaxation using two K-functions. The ratio $\tau_\alpha/\tau_{JG}$ increases with decreasing $l$ or increasing inter-bead interaction because $\sigma$ is fixed at 4.0 Å. Data in figure are from Ref. [13], and replotted as a new figure.

The second example consists of microgel particles that can be made soft, intermediate, and stiff, and naturally inter-particle interaction increases in this order. Figure 2(a) shows $\beta \equiv (1-n)$ obtained from fits to correlation obtained by light scattering experiments.[14] Again we have $n$ increasing with increasing inter-particle interaction.

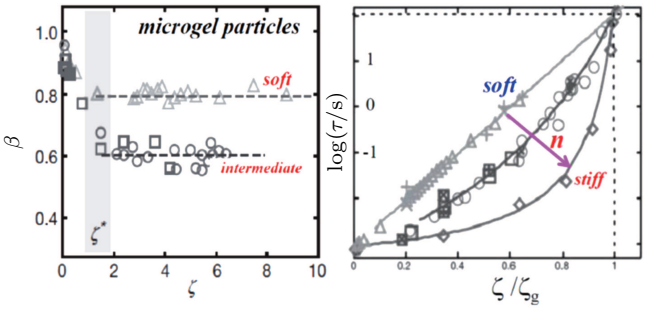



**Fig. 2.** (color online) (a) Plot of $\beta \equiv (1-n)$ vs. volume fraction $\zeta$ of stiff (95 nm), intermediate (92 nm and 168 nm), and soft (80 nm) microgels. (b) $\log\tau_\alpha$ vs. $\zeta/\zeta_g$ for the stiff, intermediate, and soft microgels, where $\tau_\alpha(\zeta_g) = 100$ s. Figures taken from Ref. [14]. Reprinted by permission from Macmillan Publishers Ltd.

The third example is the small molecular glassformer, quinaldine (QN).[15] Pure QN has weak intermolecular interaction as reflected by its low glass transition temperature $T_g$ and the narrow dielectric loss peak fitted by $n = 0.28$ in Fig. 3. Interaction of QN is increased by mixing QN with oligomers of polystyrene with higher $T_g$. There is corresponding increase of $n$ of the K-function used to fit broader loss peak of QN in the mixtures. Moreover, $n$ increases with increasing $T_g$ of the PS oligomers.

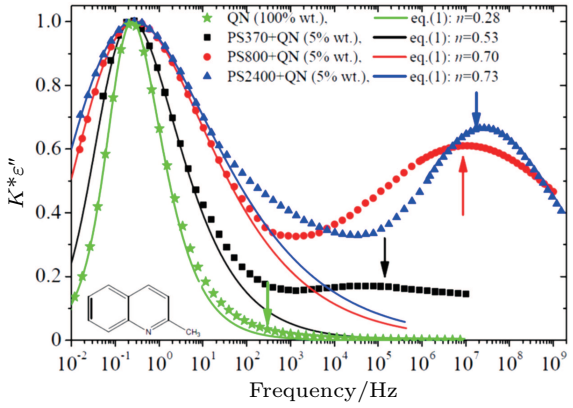



**Fig. 3.** (color online) Normalized dielectric loss vs. frequency for spectra with the same peak frequency of pure quinaldine (QN) (green stars, $T = 186$ K) and QN dissolved at 5% concentration in oligostyrene with $M_w = 370$ g/mol (black squares, $T = 233$ K), $M_w = 800$ g/mol (red circles, $T = 268$ K), $M_w = 2400$ g/mol (blue triangles, $T = 321$ K). Green, black, red and blue lines are fits by K-functions with $n = 0.28$, 0.53, 0.70, and 0.73 respectively. Data in figure are from Ref. [15] and replotted.

### 2.2. Universal properties originate from $n$

Thermodynamic variables pressure $P$ and temperature $T$ and their conjugate variables volume $V$ and entropy $S$ definitely influence the structural $\alpha$-relaxation time $\tau_\alpha$. Conventional theories of glass transition such the free volume model[16] and the configurational entropy model[17] put emphasis solely on the thermodynamic variables, neglecting the effects coming from the many-body relaxation. Current theories including the mode coupling theory[18,19] and the random first order transition (RFOT) theory[20] have not dealt with the many-body relaxation directly either. This is an oversight in view of the experimental data on many small molecular, polymeric, and ionically conducting glassformers, showing that the frequency dispersion or $n$ not only controls many other properties, but also is invariant to widely different combinations of $P$ and $T$ as long as $\tau_\alpha$ is kept constant.[11,21–23] Three examples are given by Figs. 4–6.

The first example is the dielectric loss spectra of 10% QN in tristyrene obtained at different $T$ and $P$ combinations but for the same $\tau_\alpha = 0.67$ s (Fig. 4).[23] The spectra superpose well, and the $\alpha$-loss peaks are well fitted by the K-function with $n = 0.53$. Since the density of the system can change a lot over the various combinations of $P$ and $T$, the invariance of $n$ is evidence of the contribution of many-body relaxation in determining not only the frequency dispersion, but also $\tau_\alpha$ and its properties. The secondary $\beta$-relaxation loss peaks at higher frequencies also maintain the same peak frequency, albeit the intensity changes somewhat. The arrow indicates the primitive frequency $f_0 = 1/\tau_0$ calculated by use of the CM Eq. (1) from $\tau_\alpha$ with $t_c = 2$ ps appropriate for van der Waals glass-formers[11] as in the present case.

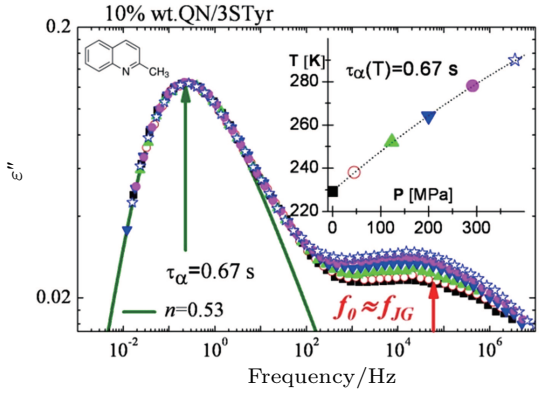



**Fig. 4.** (color online) $T$–$P$ superposition of loss spectra for 10% QN in tristyrene at different $T$ and $P$ shown in the inset but at same $\tau_\alpha = 0.67$ s. The line is fit by the K-function with $n = 0.53$. The results demonstrate the co-invariance of three quantities $\tau_\alpha$, $n$, and $\tau_{JG}$. Reprinted with permission from Ref. [23]. Copyright (2012) American Chemical Society.

The second example is taken from ionic conductivity relaxation of a room temperature ionic liquid, [Si-MIm][BF4].[24] Keeping the conductivity $\alpha$-relaxation time $\tau_\alpha$ constant in Fig. 5, the electric modulus spectra taken at two different combinations of $P$ and $T$ show the $\alpha$-relaxation loss peak superpose well, and are well fitted by the K-function with $n = 0.43$.[24] Although this ionic liquid is glass-forming when temperature is lowered, shown here is the ionic conductivity relaxation, which is decoupled from the structural $\alpha$-

relaxation and yet its frequency dispersion is invariant to variations of $P$ and $T$ if $\tau_\alpha$ is kept constant.

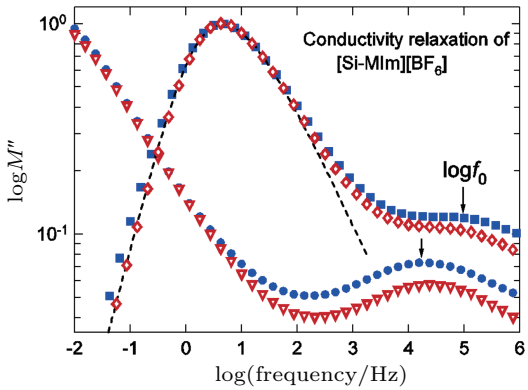



**Fig. 5.** (color online) Normalized $M(f)$ spectra of ionic liquid [Si-MIm][$BF_4$] at different $P$ and $T$ to show co-invariance of $\tau_\alpha$, $\tau_\beta$, and $n$ at constant $\tau_\alpha$. Blue squares and circles ($P = 0.1$ MPa, $T = 218$ K and 208 K from right to left). Red diamonds and triangles ($T = 253$ K, $P = 300$ MPa and 500 MPa from right to left. Dashed line is fit by the K-function with $n = 0.43$. The arrows indicate log of the primitive frequencies $f_0 \equiv 1/2\pi\tau_0$, with $\tau_0$ calculated by Eq. (1). Data are taken from Ref. [24] and redrawn here.

The 3rd example is taken from the bead-necklace model of polymer, the TACF of which has been shown before in Fig. 1. Here the parameters are fixed with $l = 1.5$ Å and $\sigma/l = 2.7$.[13] For two different fixed values of $\tau_\alpha$, figure 6 shows that the time dependence of the slower $\alpha$-relaxation is unchanged on varying the combinations of $P$ and $T$.

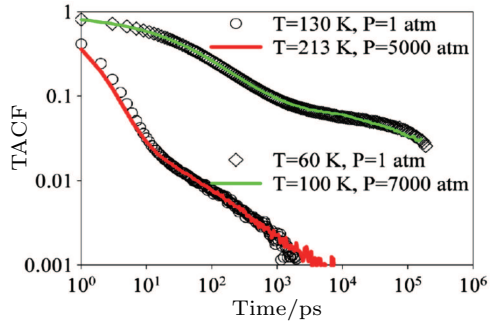



**Fig. 6.** (color online) TACF obtained from simulations of melts with $l = 1.5$ Å ($\sigma/l = 2.7$) at different temperature and pressure as shown. Reprinted with permission from Ref. [23].

## 2.3. The primitive relaxation is fundamental to universal properties

The many-body relaxation and diffusion with correlation function described by the K-function are the end product of the evolution of dynamics with time. Starting initially from the simplest one-body relaxation/diffusion process, increasing number of units participate in the relaxation or diffusion process with time. From this time evolution of the dynamics from one-body to many-body, one may expect the existence of connection between the relaxation time $\tau_0$ of the one-body process and $\tau_\alpha$ of the final many-body process. Such a connection is given by the CM in the form of Eq. (1). This connection between $\tau_0$ and $\tau_\alpha$ is quantitative provided that the values of $n$ and $t_c$ are known from experiments. For van der Waals molecular and polymeric glassformers, $t_c = 1$–$2$ ps. Since $t_c$ depends solely on the interaction and not on the other variables, $P$, $T$, $\lambda, \ldots$. The connection between the two different dependences of $\tau_0$ and $\tau_\alpha$ on any variable $\lambda$ takes the form

$$\tau_\alpha(\lambda) \propto [\tau_0(\lambda)]^{1/(1-n)}. \tag{2}$$

The dependence of $\tau_0$ on $\lambda$ is often simple and known because of the absence of many-body effects. According to Eq. (2), the dependence of $\tau_\alpha$ on $\lambda$ is stronger than $\tau_0$, and hence may appear abnormal. An example is the scattering vector $Q$-dependence of $\tau_\alpha$ observed by neutron scattering in polymers, and light scattering in colloidal particles.[11,12] While it is well known that $\tau_0(Q) \propto Q^{-2}$ and verified by experiment, the dependences of $\tau_\alpha$ on $Q$ found is close to $\tau_\alpha(Q) \propto Q^{-2/(1-n)}$. This is an universal property because the same $Q^{-2/(1-n)}$-dependence of the many-body relaxation time was found by dynamic light scattering in non-glassforming systems including semidilute polymer solutions and polymer cluster solutions.[11]

Empirically $\tau_\alpha$ is a function of the product variable $\rho^\gamma/T$, where $\rho$ is the density and $\gamma$ a constant with value dependent on the glass-former.[25,26] The CM equations (1) and (2) require that $\tau_0$ is also a function of the same thermodynamic product variable $\rho^\gamma/T$. The interesting question is where does the dependence on $\rho^\gamma/T$ originate, $\tau_\alpha$ or $\tau_0$? From the chronological description of the CM, it is clear that the primitive relaxation comes first, and hence the dependence on $\rho^\gamma/T$ starts with its relaxation time $\tau_0$. After the onset of chaos and subsequent development of many-body dynamics, $\tau_\alpha$ inherits the dependence on $\rho^\gamma/T$. Experimental support of this conclusion will be given in Subsection 2.3.2. This simple result from the CM has tremendous impact on how the dependence on temperature and density should be introduced in theory of glass transition. Theories that introduce the dependence on $\rho^\gamma/T$ through $\tau_\alpha$ without tracing its origin to $\tau_0$ are contradicting casuality and the simple result from Eq. (1) of the CM.

### 2.3.1. Support from the JG $\beta$-relaxation

The primitive relaxation is the precursor of the many-body $\alpha$-relaxation, and it is analogous to the secondary relaxation that involves the motion of the entire molecule or repeat unit in the case of polymers. To distinguish this special kind of secondary relaxation from trivial ones that involve only a part of the molecule, we have called them Johari–Goldstein (JG) $\beta$-relaxations.[11,27,28] We chose this nomenclature for this special kind of secondary relaxations also for the purpose of honoring our colleagues, Johari and Goldstein for their discovery more than 4 decades ago that totally rigid small molecules like chlorobenzene and toluene can have a secondary relaxation,[29,30] and of course they belong to the special class because any motion of totally rigid molecule must

involve the entire molecule. However, it must be made clear that the discovery of the special class of secondary relaxations having strong connections to the $\alpha$-relaxation originates from Refs. [27] and [28] and is based on the precept of the coupling model,[11] and not from either Johari or Goldstein at any time in the past.

The JG $\beta$-relaxation appears at shorter times or higher frequencies than the $\alpha$-relaxation in Figs. 1–6. Several properties of the JG $\beta$-relaxation time $\tau_{\rm JG}$ are in accord with $\tau_0$, in support of the approximate equality $\tau_{\rm JG} \approx \tau_0$. Firstly, in Figs. 3–5 where all vertical arrows drawn indicate either $\tau_0$ (or $f_0 = 1/2\pi\tau_0$) calculated by Eq. (1) from the known values of $\tau_\alpha$, $n$, and $t_{\rm c}$, there is good agreement between the observed $\tau_{\rm JG}$ (or $f_{\rm JG}$) and the calculated $\tau_0$ (or $f_0$). Secondly, the observed increasing separation of $\tau_\alpha$ from $\tau_{\rm JG}$ on increasing $n$ and shown in Figs. 1 and 3 is in accord the same trend predicted by Eq. (1) on the separation between $\tau_\alpha$ and $\tau_0$. Thirdly, figures 4–6 demonstrate the co-invariance of three quantities $\tau_\alpha$, $n$, and $\tau_{\rm JG}$ to widely different combinations of $T$ and $P$, which is the same as the co-invariance predicted for $\tau_\alpha$, $n$, and $\tau_0$ by Eq. (1). All are universal properties because they are found generally in many glass-formers.[11,21]

Like the primitive relaxation of the CM, the JG $\beta$-relaxation is the origin or the precursor of the $\alpha$-relaxation, and hence the latter would not exist without the former taking place at earlier time. For this reason, the JG $\beta$-relaxation is present in all glass-formers, although it may be difficult to be resolved and unambiguously detected by experiment and simulations. The difficulty is because the JG $\beta$-relaxation is more local, and its relaxation strength is smaller than or in some cases even negligible compared with that of the many-body $\alpha$-relaxation. The JG $\beta$-relaxation's connections to the $\alpha$-relaxation indicate its fundamental importance. It is a mistake to ignore the JG $\beta$-relaxation in considering any property of the $\alpha$-relaxation, and in constructing a theory of glass transition. Unfortunately, this malpractice continues to the present time despite the volume of experimental evidences showing that its role cannot be neglected.

Notwithstanding the difficulty caused by its small relaxation strength, the JG $\beta$-relaxation was found in many small molecular, polymeric, inorganic,[11,27,28,31] plastic crystalline,[32,33] polymer blends,[34] and metallic glasses,[35–38] as well as in room temperature ionic liquids,[24] amorphous pharmaceuticals,[39] carbohydrates,[40,41] aqueous mixtures,[42,43] and hydrated proteins.[44–46] The ubiquitous JG $\beta$-relaxation is another one of the universal properties of glass-forming substances and systems.

### 2.3.2. $\tau_\alpha$ and $\tau_{\rm JG}$ are different function of the same variable $\rho^\gamma/T$

To accentuate this universal property of strong connection between $\tau_\alpha$, $n$, and $\tau_{\rm JG}$, once more, we show in Fig. 7 that $\tau_\alpha$ and $\tau_{\rm JG}$ of DGEBA (diglycidyl ether of bisphenol-A) with $M_{\rm w} = 380$ g/mol are simultaneously functions of the same thermodynamic scaling variable, $\rho^\gamma/T$, with $\gamma = 3.5$. There is also good agreement between $\tau_{\rm JG}$ and $\tau_0$ calculated at several state points by Eq. (1) with $(1-n) = 0.52$ obtained by fitting the $\alpha$-relaxation by the K-function.[47]

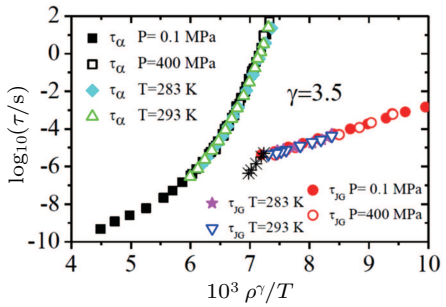



**Fig. 7.** (color online) log of $\tau_\alpha$ and $\tau_{\rm JG}$ of DGEBA obtained isobarically as function of $T$ and isothermally as function of $P$ plotted together vs. $\rho^\gamma/T$. Black asterisks: values of $\log_{10}(\tau_0)$ at several state points calculated by Eq. (1) with $(1-n) = 0.52$ obtained by fitting the $\alpha$-relaxation by the K-function. Reproduced from Ref. [47] by permission.

Molecular dynamics simulations of binary Lennard–Jones liquids were performed[48] with the exponent of the attractive part of the potential fixed at the value of 6 and the exponent $p$ of the repulsive part varied over the values of 8, 12, 24, and 36. The diffusion coefficients for the simulated liquids in normal and moderately supercooled states are a unique function of the variable $\rho^\gamma/T$. The value of $\gamma$ turns out to be determined by the steepness of the repulsive part of $U(r)$ in the region bounded by $r_{\rm c}$ and $r_{1/2}$, where $r_{\rm c}$ is the closest approach distance between the larger particles and $r_{1/2}$ is the separation distance between the larger particles corresponding to the half-height of the pair distribution functions, $g(r)$. Within the range $r_{\rm c} < r < r_{1/2}$, the distance is smaller than the average separation between the larger particles of the binary L–J liquids. At such short distances, where $\gamma$ is determined mainly albeit not totally by the repulsive part of $U(r)$, it is the primitive relaxation or the local JG $\beta$-relaxation that is more directly related to the repulsive part of $U(r)$ than the cooperative $\alpha$-relaxation, which involves more particles and longer length scale. Thus, this is evidence that the dependence on $\rho^\gamma/T$ of dynamic quantity related to structural relaxation originates from the JG $\beta$-relaxation or the primitive relaxation of the CM.[11] This original dependence of $\tau_{\rm JG}$ (or $\tau_0$) on $\rho^\gamma/T$ or $T^{-1}V^{-\gamma}$, where $V$ is the specific volume, is passed onto $\tau_\alpha$ of the structural $\alpha$-relaxation and magnified in $\tau_\alpha$ at later time through action of the many-body dynamics. Additional confirmation can be found from recent papers.[47] The results show the fundamental role of the primitive or JG $\beta$-relaxation, and also the importance of recognizing that many-body relaxation has its own separate effect on $\tau_\alpha$ and glass transition, distinguishable from the effect due to the change of temperature and pressure. Theories of glass transition that are based solely on

the $\alpha$-relaxation and consider only changes of density and entropy cannot be correct because of the neglect of the primitive or JG $\beta$-relaxation and failure in incorporating many-body nature of the structural $\alpha$-relaxation and the effects it has on $\tau_\alpha$.

## 3. The universal primitive relaxation

The primitive relaxation could be overlooked or viewed by some workers as merely a construct of the CM and has no real manifestation in experiment. This wrong impression can still hold despite the generally good correspondence between the calculated primitive relaxation time $\tau_0$ and the experimentally observed $\tau_{JG}$.[11,21–24,27,28,31–34,38–41] Notwithstanding, experiments can be carried out to directly observe the primitive relaxation by reducing the many-body relaxation to one-body relaxation when $n \to 0$. One can check if the observed relaxation time is the same or nearly the same as $\tau_0 \approx \tau_{JG}$ as predicted by Eq. (1) of the CM. The experiments I have in mind are on glassformers with dimension or dimensions reduced in size down to nanometer length scale. The small size of the sample practically makes many-body process with larger length scale impossible, particularly at and near the surface and interface, resulting in the observation of the primitive relaxation.

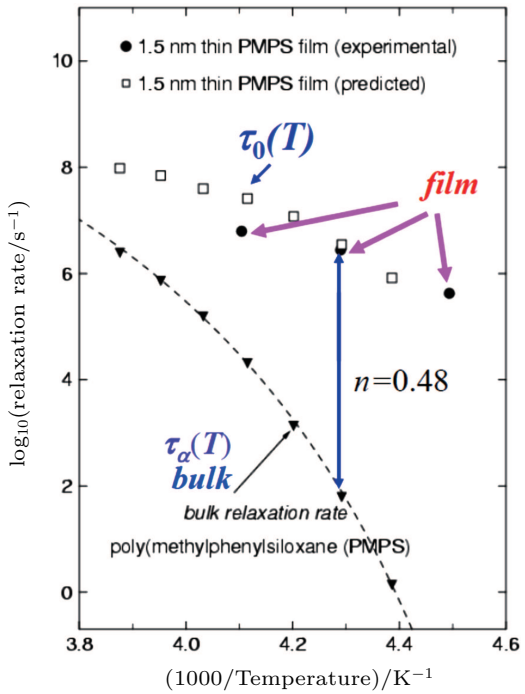



**Fig. 8.** (color online) Plot of $\log \tau_\alpha$ of PMPS observed in bulk (closed triangles) and in 1.5 nm thin films (closed circles). Open squares indicate the values of $\log_{10}(\tau_0)$ calculated by Eq. (1) with $(1-n) = 0.52$ obtained by fitting the $\alpha$-relaxation of bulk PMPS by the K-function.

One example is the ultrathin films of poly (methylphenylsiloxane) (PMPS) with thickness of $\approx 1.5$ nm confined within the galleys of nanocomposites.[49] Figure 8 shows the $\tau_\alpha$ of poly(methylphenylsiloxane) (PMPS) observed in the bulk and in 1.5 nm thin films. There is about 6 orders of magnitude reduction of $\tau_\alpha$ in the thin film compared with the bulk at the lowest temperature above $T_g$ of bulk PMPS shown in the figure. There is good agreement between $\tau_\alpha$ observed in the thin film and the values of $\log_{10}(\tau_0)$ calculated by Eq. (1) with $(1-n) = 0.52$ obtained by fitting the $\alpha$-relaxation of bulk PMPS by the K-function.[50–52] The results from this experiment clearly demonstrate that the primitive relaxation can be observed directly after suppressing many-body aspects of the relaxation and when $n \to 0$.

The same effect was obtained by confining ortho-terphenyl (OTP)[53,54] and poly(dimethylsiloxane) (PDMS) in silanized glass pores.[55,56] Negative pressure could be present in the case of OTP as pointed out in Ref. [53], making the confined OTP less dense and weakening the interaction strength as well. This situation acts in concert with the finite size effect to lead to $n \to 0$.[54] In both OTP[54] and PDMS,[52] it was found that $\tau_\alpha \to \tau_0$. The results of nano-confined PDMS are presented in Fig. 9, where $f_\alpha \equiv (1/2\pi\tau_\alpha)$ can be seen to approach $f_0 \equiv (1/2\pi\tau_0)$ as the pore size becomes smaller.

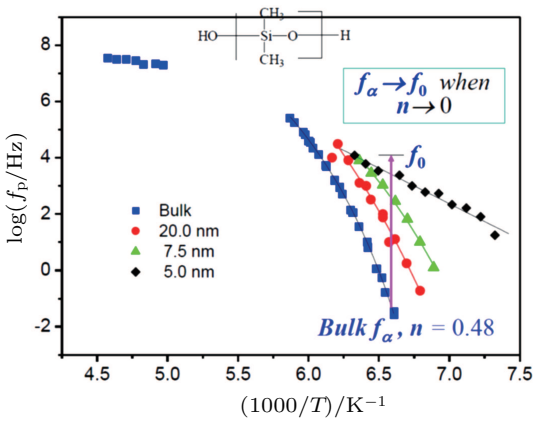



**Fig. 9.** (color online) Dielectric $\alpha$-loss peak frequency of bulk and nano-confined PDMS vs. $1000/T$. $f_0 \equiv (1/2\pi\tau_0)$ at one temperature is calculated by Eq. (1) with $n = 0.48$ obtained from fit to loss spectra of bulk PDMS by the K-function. Data digitized from Ref. [55] to construct the new figure.

Without using artificial walls to confine, self nano-confinement of alkyl chains occurs naturally in nano-domains formed as a result of nanophase separation of incompatible main and side-chain parts in higher members of poly(*n*-alkyl methacrylates) (P*n*AMA). Alkyl groups in the side chains of the polymer aggregate in the melt and form self-assembled alkyl nanodomains.[57,58] A polyethylene-like glass transition called $\alpha_{PE}$ occurs within the alkyl nanodomains, and the associated $\tau_\alpha$ is shown in Fig. 10. The size of the nanodomains decreases with the number, $C$, of alkyl carbon atoms per side chain of P*n*AMA, from 2 nm for $C = 10$ in poly(*n*-decylmethacrylate) to 1 nm for $C = 4$ in poly(*n*-butylmethacrylate). The $\tau_\alpha$ of $C = 10$ nanodomains has the Vogel–Fulcher $T$-dependence like in bulk glass-formers. In

contrast, $\tau_\alpha$ in $C = 4$ nanodomains becomes much shorter and assumes the Arrhenius $T$-dependence. It is likely that $n \to 0$ in the smallest $C = 4$ nano-domain, and $\tau_\alpha$ becomes the same as $\tau_0$. If so, $\tau_\alpha$ of $C = 4$ nanodomains also could be the same as the JG $\beta$-relaxation time $\tau_{JG}$ of $C = 10$ nanodomains. This expectation was verified in experiment by rapid quenching of the $C = 10$ sample.[59] The procedure enabled the JG $\beta$-relaxation to be resolved, and its $\tau_{JG}$ is nearly the same as $\tau_\alpha$ of $C = 4$ nanodomains shown in Fig. 10.

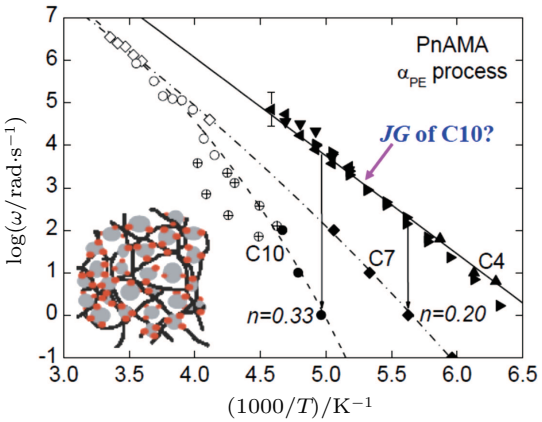



**Fig. 10.** (color online) Arrhenius plot for $\tau_{C,PE}$ of $\alpha_{PE}$ processes in higher P$n$AMA with $C = 4$ (triangles), $C = 7$ (diamonds), and $C = 10$ (circles). Dielectric (full symbols), shear (open symbols), and heat capacity ($\oplus$) are shown. The lines are VF fits for $C = 7$ and $C = 10$, and Arrhenius fit for $C = 4$. The inset depicts nanophase separation in P$n$AMA.

Recently, Zhu *et al.*[60] used the method of surface grating decay and successfully measured the surface diffusion on an organic glass-former, indomethacin (IMC), for the first time. They found that surface diffusion coefficient $D_S$ is about $10^6$ times larger than bulk $D_V$ at temperatures around $T_g$. This large difference between $D_S$ and $D_V$ is brought out in Fig. 11 where $\log(1/D_S)$ and $\log(1/D_V)$ have been shifted by $-17.5$ to bring $\log(1/D_V)$ to coincide with $\log\tau_\alpha$ of bulk IMC near its $T_g$ determined by dielectric relaxation and also by DSC. The value of $n = 0.41$ of bulk IMC was obtained by fitting dielectric relaxation spectra by the K-function.[61] The primitive $\tau_0$ calculated by Eq. (1) from $\tau_\alpha$ of bulk IMC is also shown Fig. 11. Assuming $n \to 0$ at the free surface, the relaxation time $\tau_s(T)$ at the surface becomes identical to the primitive relaxation time $\tau_0(T)$. It can be seen that the calculated $\tau_0$ and hence the predicted $\tau_s(T)$ are shorter than the bulk $\tau_\alpha$ also by about six orders of magnitude in a range of temperature near and below the bulk $T_g$, in accord with the difference between $D_S$ and $D_V$. The primitive $\tau_0(T)$ used to estimate $\tau_s(T)$ is calculated from the bulk $\tau_\alpha(T)$, and hence is for the bulk only. At the surface with free space available, $\tau_0(T)$ can be shorter than the calculated bulk value. This effect at the surface can increase the ratios $\tau_\alpha(T_g)/\tau_s(T_g)$ and $D_V(T_g)/D_s(T_g)$. On the other hand, there is decoupling of $D_V(T)$ from $T/\eta$ less than two orders of magnitude at $T = T_g$, which causes a reduction of the enhancement in $D_V(T_g)/D_s(T_g)$ estimated by $\tau_\alpha(T_g)/\tau_s(T_g)$. The balance of two opposing effects has to be taken into consideration in conjunction with the estimate $\tau_\alpha(T_g)/\tau_s(T_g)$ in determining the actual enhancement of mobility at the surface.

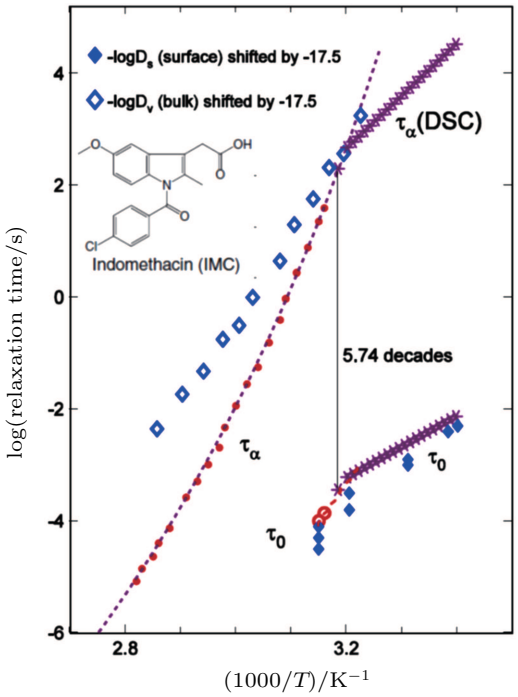



**Fig. 11.** (color online) $\alpha$-relaxation time $\tau_\alpha$, (red filled circles together with the VFT fit (dashed purple line)). The purple asterisks on top are $\tau_\alpha$ from DSC measurements. The first asterisk on the upper left corresponds to $\tau_\alpha = 200$ s at 315 K. The rest of the asterisks represents $\tau_\alpha$ in the glassy state. Lower part: the red open circles together with the red dashed line are the calculated primitive relaxation time $\tau_0$ from $\tau_\alpha$. The purple asterisks at the bottom are the $\tau_0$ calculated from $\tau_\alpha$ obtained by DSC. The vertical line indicates $(\log\tau_\alpha - \log\tau_0) = 5.74$ decades at $T_g = 315$ K. The open and closed blue diamonds are $\log(1/D_v)$ and $\log(1/D_s)$ data shifted downward by 17.5 decades to place $\log(1/D_v)$ at approximately the same locations as $\log\tau_\alpha$. Note that the same shift superpose $\log(1/D_s)$ to $\log\tau_0$.

Another van der Waals glass-former ortho-terphenyl (OTP) has a larger value of $n = 0.50$.[62] The same operation leads to the prediction of a larger value of $\log[\tau_\alpha(T_g)/\tau_s(T_g)] = 7.2$, which approximately matches the observed value of $\log[D_v(T_g)/D_s(T_g)]$ in surface grating decay experiment.[62] If the same experiment was done on another van der Waals glass-former without complication of hydrogen bonds and value of $n$ smaller than IMC, smaller $\tau_\alpha(T_g)/\tau_s(T_g)$ and $D_v(T_g)/D_s(T_g)$ than observed in IMC are predicted. A candidate for such future experiment is propylene carbonate with smaller value of $n = 0.27$.[31]

Metallic alloys have chemical and physical structures so different from molecular glass-formers and yet their structural $\alpha$-relaxation, the JG $\beta$-relaxation, and the caged dynamics of metallic glasses are remarkably similar in properties. Thus it is consequential to study the surface mobility of metallic glasses and compare the results with molecular glass-formers

like IMC and OTP. Indeed measurements of surface diffusion of the canonical metallic glass, $Pd_{40}Cu_{30}Ni_{10}P_{20}$, were carried out by the surface grating method to make direct comparison with the molecular glass-formers.[63] The coupling parameter $n$ of $Pd_{40}Cu_{30}Ni_{10}P_{20}$ is 0.46, obtained from the fit to the shear loss modulus data by the Kohrausch function with stretch exponent $\beta_K \equiv (1-n) = 0.54$. The $t_c \approx 0.2$ ps for metallic systems deduced from simulations[64,65] is shorter than 1–2 ps for soft molecular glass-formers and polymers. This difference is reasonable in view of the stronger interaction of metal atoms compared with van der Waals interaction in soft matter, as exemplified by the much higher shear modulus of metallic glasses than molecular glasses. Again with the choice of $\tau_\alpha(T_g) = 10^3$ s, and the values of $t_c \approx 0.2$ ps and $n = 0.46$, the CM gives $\log[\tau_\alpha(T_g)/\tau_s(T_g)] = 7.2$,[66] which is about one order of magnitude smaller than the experimental value of $\log[D_v(T_g)/D_s(T_g)]$.

Measurements of Ag radiotracer diffusion in shear bands of deformed bulk metallic glass, $Pd_{40}Ni_{40}P_{20}$,[67] have found a colossal enhancement of diffusion coefficient by more than eight orders of magnitude than in undeformed $Pd_{40}Ni_{40}P_{20}$. Suggestion was made by Bokeloh *et al.*[67] that enhanced diffusion occurs in high-mobility pathways originating from some excess free volume distribution inside the shear bands. The use of the CM together with the values of $t_c \approx 0.2$ ps and $n = 0.50$ known from mechanical measurements allow quantitative calculation of the maximum of the enhancement of diffusivity, again from $\tau_\alpha(T)/\tau_0(T)$, possible in high-mobility pathways of the shear bands.[68] Within the range of eight to ten orders of magnitude, the calculated maximum enhancement is capable to account for the experimental observation.

The cause of the fast surface diffusion is the nearly vanishing of intermolecular coupling of relaxation and diffusion, i,e, $n \to 0$, at the surface. Thus, surface diffusion experiment is another way to reveal the primitive diffusion of IMC, OTP, and $Pd_{40}Cu_{30}Ni_{10}P_{20}$, and show that it is real and an universal feature of the dynamics.

## 4. Universal properties in non-glassforming systems

To heighten the awareness of the reader that universal properties of many-body relaxation and diffusion are manifested in all interacting systems and not just glassformers, some examples are given in this section. More can be found in Ref. [11]. I shall continue on the themes of the previous sections on crossover at $t_c$ and the quantitative connections between the many-body $\tau_\alpha$ and the primitive $\tau_0$, as well as the revelation of $\tau_0$ by nano-confinement.

### 4.1. Yttria stabilized zirconia

The first example is taken from oxygen ion conductivity relaxation in yttria stabilized zirconia (YSZ), $ZrO_2$:$x$%$Y_2O_3$, with its structure depicted in Fig. 12.

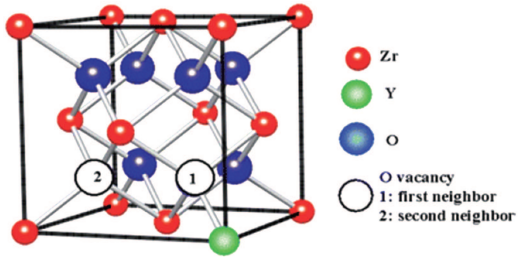



**Fig. 12.** (color online) Structure of YSZ.

One of the universal properties exhibited by YSZ with $x$ ranging from 8 to 10 is the crossover from primitive oxygen ion conductivity relaxation to many-body conductivity relaxation at $t_c \approx$ 1–2 ps. This is evidenced in Fig. 13 by the change of the activation energy of d.c. conductivity $\sigma$ from $E_a = 0.49$ eV to $E_a^* = 1.16$ eV at the level of $\sigma$ corresponding to conductivity relaxation time (calculated from the Maxell relation) of about 1 to 2 ps as indicated in the figure. $E_a$ and $E_a^*$ are also respectively the activation energies of the primitive conductivity relaxation time $\tau_0$ and the many-body conductivity relaxation time $\tau^*$. The relation,

$$E_a^* = (1-n)E_a, \tag{3}$$

is a corollary of Eq. (1). It is verified (see Fig. 13) since $n = 0.57$ is known already from the fit of the electric modulus spectra by the K-function.[69]

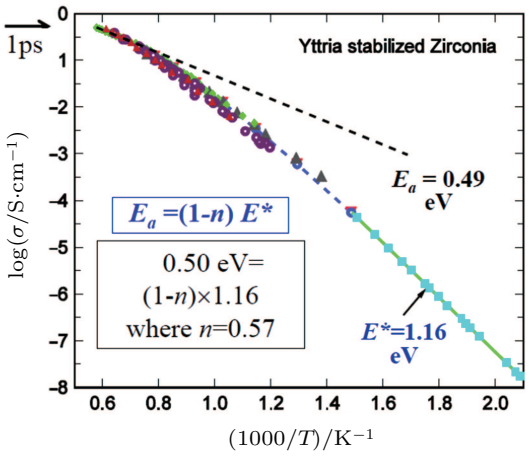



**Fig. 13.** (color online) Change of activation energy of conductivity $\sigma$ from $E_a = 0.49$ eV to $E_a^* = 1.16$ eV when the relaxation time crosses $t_c \approx 1$ to 2 ps. The arrow indicates the level of $\sigma$ where the relaxation time is 1 ps.

Conductivity in thin films of YSZ on MgO substrate has been measured.[70] On reducing the film thickness, figure 14 shows $\sigma$ increases and its activation energy decreases. The effect is caused by the much higher conductivity of the surface making more important contribution in thinner films.[70]

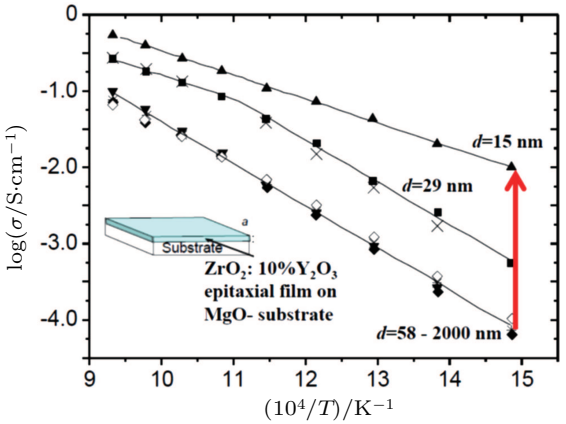



**Fig. 14.** (color online) $T$-dependence of the electrical conductivity determined for epitaxial YSZ thin films on MgO as substrate with different thicknesses. The red vertical arrow indicates the roughly 2 orders of magnitude change at the same value of the reciprocal temperature as in Fig. 15. Data points digitized from Ref. [70] and plotted in this new figure.

The data of $\sigma$ in YSZ film 15 nm thick are converted to conductivity relaxation time $\tau^*$ (15 nm) by the Maxwell relation and compared with the many-body conductivity relaxation time $\tau^*$ of bulk YSZ in Fig. 14. Also plotted in the figure is the primitive $\tau_0$ calculated from $\tau^*$ with $n = 0.57$ and $t_c \approx 2$ ps. It can be seen by inspection that $\tau^*$ (15 nm) is nearly the same as the calculated $\tau_0$, showing once more that $\tau_0$ can be directly observed via the surface conductivity contribution due to vanishing of inter-ionic coupling and $n \to 0$.[69]

Another universal property of many-body relaxation and diffusion can be elucidated by the experimental data shown in Fig. 15.[69] At lower temperatures before the crossover, the temperature dependence of $\tau^*$ of bulk YSZ is Arrhenius and given by $\tau^* = \tau^*_\infty \exp(E^*_a/kT)$, where $\tau^*_\infty$ is the prefactor and $E^*_a = 1.16$ eV. The intercept of the Arrhenius fits to $\tau^*(T)$ with the $y$-axis at infinite temperature gives the prefactor $\tau^*_\infty = 10^{16.44}$ s, which is much shorter than the oxygen vibrational time given by the reciprocal of the angular frequency $\omega_{vib}$ corresponding to the narrow band at 690 cm$^{-1}$ of the hyper-Raman spectra shown in the inset. On the other hand, the intercept of the Arrhenius $T$-dependence of $\tau_0(T)$ with the $y$-axis yields the prefactor $\tau_{0\infty}$ in good agreement with the oxygen vibrational time.[23]

According to Eq. (1), from the experimental Arrhenius $T$-dependence of $\tau^*$, it follows that the $T$-dependence of $\tau_0$ is also Arrhenius. When written in the form $\tau_0 = \tau_\infty \exp(E_a/kT)$, the primitive prefactor $\tau_\infty$ is related to many-body $\tau^*_\infty$ by

$$\tau^*_\infty = [(t_c)^{-n}\tau_\infty]^{1/(1-n)}, \tag{4}$$

which is a result in parallel with $E^*_a = (1-n)E_a$ and considered before in Fig. 13. The $\tau_\infty$ calculated from $\tau^*_\infty$ with $t_c = 2$ ps and 1 ps agrees with $\omega_{vib}$ from hyper-Raman experiment. The success of relating the anomalous $E^*_a$ and $\tau^*_\infty$ to one-body $E_a$ and $\tau_\infty$ by Eqs. (3) and (4) via the same $n$ is another proof of the ability of the CM to account for many-body relaxation.

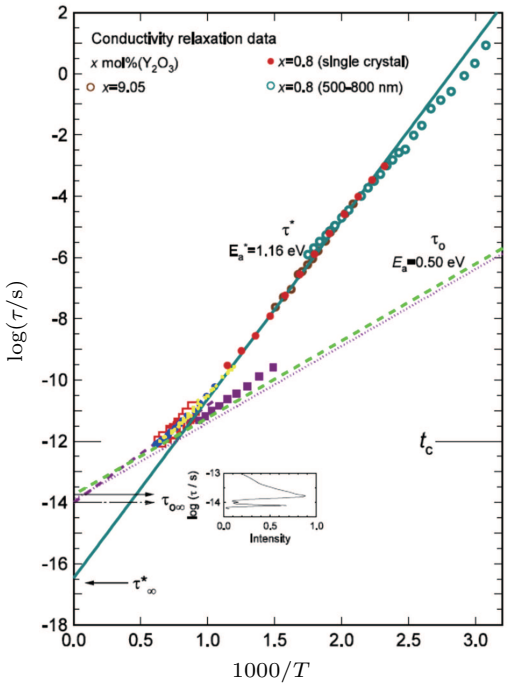



**Fig. 15.** (color online) Arrhenius plots of various relaxation time of oxygen ions in bulk YSZ and thin films of YSZ. The data of the conductivity relaxation times, $\tau^*(T)$, of 15 nm YSZ thin film deposited on MgO in Fig. 14 are shown by closed purple squares. The length of the red arrow of about 2 decades has the same length and located at the same temperature as the one in Fig. 14. The conductivity relaxation time $\tau^*(T)$ was obtained in bulk YSZ samples. The thicker solid lines are Arrhenius fits to the data of $\tau^*$. The thinner broken and dotted lines are the $\tau_0(T)$ calculated from $\tau^*(T)$ with $t_c = 2$ ps and 1 ps, respectively. The intercepts of the Arrhenius fits to $\tau^*(T)$ with the $y$-axis at infinite temperature give the prefactors $\tau^*_\infty = 10^{16.44}$ s. The intercept of the Arrhenius $T$-dependence of $\tau_0(T)$ yields the prefactor $\tau_{0\infty}$ in good agreement with the reciprocal of the angular frequency corresponding to the narrow band at 690 cm$^{-1}$ of the hyper-Raman spectra shown in the inset.

Many more successful applications of the CM to explain the ion dynamics in other ionic conductors can be found in the two book.[11,12]

### 4.2. Monoclinic phase II of 2-adamantanone

The anomalous activation energy barrier $E^*_a$ and the prefactor $\tau^*_\infty$ are universal properties of many-body relaxation and diffusion processes that have Arrhenius temperature dependence. An example of these universal properties from a strikingly different system than YSZ is given here to dramatize the universality. The substance is 2-adamantanone ($C_{10}H_{14}O$), or 2A=O for short, and it is composed of simple rigid pseudoglobular molecules.[33] We are interested in its monoclinic phase II below about 180 K. As shown in Fig. 16, the structure is ordered both in translation and in orientation, and far different from the amorphous structure of conventional glassformers in either the liquid or the glassy state. There is however the existence of a statistical intrinsic disorder concerning the site occupancy of the oxygen atom. As illustrated by the picture in Fig. 16(a), the oxygen atom can occupy three possible sites[33] with temperature-independent fractional occupancies of 25% (O1 and O2) and 50% (O3).

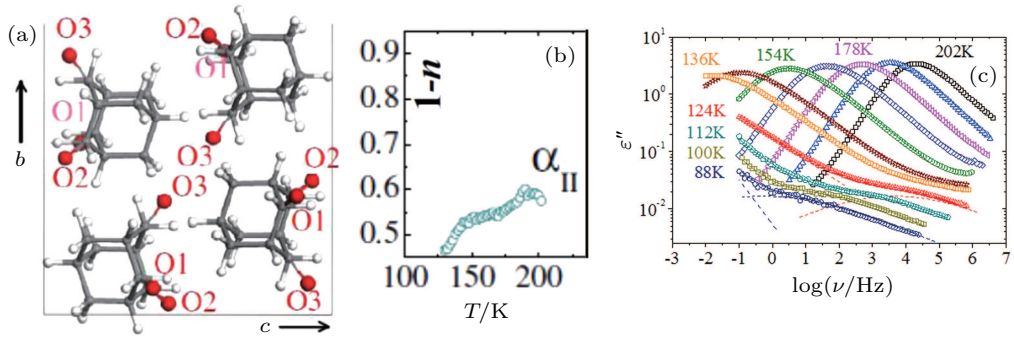



**Fig. 16.** (color online) (a) 2-adamantanone phase II with oxygen atoms (red) within their three occupational sites of the (00l) crystallographic phase of OO. Red labeled atoms correspond to the oxygen atoms within their three sites of fractional occupancies 0.25 (O1), 0.25 (O2), and 0.50 (O3). Panel (c) shows the presence of the $\alpha$-relaxation and $\beta$-relaxation in the isothermal spectra. Panel (b) presents the exponent of the K-function for different temperatures. Data from Ref. [33], and redrawn.

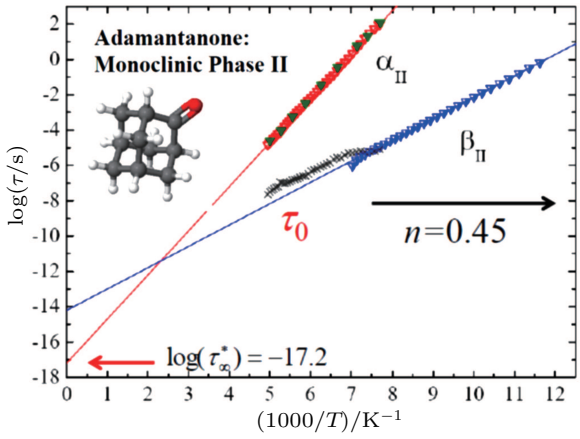



**Fig. 17.** (color online) Relaxation time as a function of reciprocal of temperature for the different relaxation processes in the orientation ordered phase II. $\alpha$-relaxation time from Refs. [24] and [25] is represented by red and green inverted triangles, respectively. $\beta$-relaxation time is shown as blue-white inverted triangles. Lines are linear regressions to data. Gray asterisks are the predicted $\tau_0$ from Eq. (1). Data from Ref. [33] and are replotted.

The statistical disorder due to the fractional occupancy of the oxygen atom enables the use of dielectric relaxation to study the dynamics of 2A=O. The isothermal dielectric loss spectra in Fig. 16(a) show the presence of a primary $\alpha$-relaxation with a considerable strength, as well as a resolved $\beta$-relaxation, which has all the properties of the JG $\beta$-relaxation, including the motion of the entire 2A=O molecule because of the rigid C=O group attached to the adamantine skeleton.[33] Figure 16(b) shows the stretch exponent, $1-n$, of the K-functions that fit the $\alpha$-loss peak. It is a function of temperature. It decreases on cooling and assumes the value of 0.46 on approaching the lower temperature at which the $\alpha$-relaxation time $\tau_\alpha$ reaches long time of 100 s as shown in Fig. 17. The temperature dependence of $\tau_\alpha$ is Arrhenius and given by $\tau_\alpha = \tau^*_\infty \exp(E^*_a/kT)$, where $E^*_a = 5746$ K and the prefactor $\tau^*_\infty$ is about $10^{-17.2}$ s. Presented in the same figure is the JG $\beta$-relaxation time $\tau_{JG}$ determined from the spectra at lower temperatures. The temperature dependence is also Arrhenius and given by $\tau_{JG} = \tau_\infty \exp(E_a/kT)$, where $E_a = 2744$ K, and $\tau_\infty$ is about $10^{-14.2}$ s. According to Eq. (3), the ratio $E_a/E^*_a$ is equal to $(1-n)$, from which we have the value of 0.48. This is close to the value of 0.46 for $(1-n)$ determined by the fit to the loss peak at lower temperatures by the K-function (see Fig. 16(c)). Using the same value of 0.48 for $(1-n)$, and substituting $\tau_\infty = 10^{-14.2}$ s and $t_c = 2$ ps into Eq. (4), we obtain the value of $10^{-16.9}$ s for $\tau^*_\infty$, close to the $10^{-17.2}$ s obtained for the prefactor of $\tau_\alpha$. Moreover, $\tau_0$ has been calculated by Eq. (1) from the experimental values of $\tau_\alpha$ and $(1-n)$ over a range of temperature. The results are shown by asterisks in Fig. 17.

The properties of the many-body molecular relaxation in 2A=O are analogous to those of the many-body ionic conductivity relaxation in YSZ, although the two systems have nothing in common except for the presence of interaction between the relaxing units. Thus, the universal properties of many-body relaxation common to both systems are engendered by interaction. The physics that gives rise to them has to be fundamental in order that it is applicable to the diverse processes and substances or systems.

### 4.3. Polymer viscoelasticity

It is worthwhile to briefly mention the application of the CM to polymer viscoelastic properties in the past three decades.[11,71–96] In particular, the applications have explained the thermo-rheological complexity of the viscoelastic spectra of amorphous polymers caused by the segmental $\alpha$-relaxation, the sub-Rouse (sR) modes, the Rouse modes, and the terminal relaxation (if the polymer is entangled) all having different coupling parameters but the primitive relaxation time of all of them, $\tau_{\alpha 0}$, $\tau_{sR0}$, and $\tau_{R0}$, share the same primitive friction coefficient $\zeta_0(T)$.[75,78,81–96] The coupling parameter $n_\alpha$ of the segmental $\alpha$-relaxation is larger than $n_{sR}$ of the sub-Rouse modes, and $n_R$ of the Rouse modes is zero. Applying the CM Eq. (1) to each of the three viscoelastic mechanisms with the same $\zeta_0(T)$ factor in $\tau_{\alpha 0}$, $\tau_{sR0}$, and $\tau_{R0}$, but different coupling parameters, the thermos-rheological complexity of polymers is explained.

The recent work[94] extends the previous one to include different dependences of $\zeta_0$ on pressure $P$, and the product

variable $TV^{\gamma}$. Again by means of the CM Eq. (1), the results explain the piezo-rheological complexity, and the $TV^{\gamma}$-rheological complexity of polymers. The viscoelastic anomalies observed experimentally are fundamental and deserve attention from the polymer physics community. Some authors rationalized the thermorheological complexity of polymers by the spatially heterogeneous segmental $\alpha$-relaxation.[97,98] This rationalization is invalid as demonstrated later on in Subsection 5.2 and in Ref. [99]. So far, only the CM can rationalize the origin of these complexities and explain some of the data quantitatively.[94]

This CM explanation of bulk viscoelastic property was extended to freestanding polymer thin films to address the changes observed on decreasing the film thickness by McKenna and coworkers.[100,101] Due to the presence of the two surfaces, the finite size effect, and the induced orientation of the entangled chains altogether reduce the coupling parameters $n_{\alpha}$ and $n_{\rm sR}$ of the segmental $\alpha$-relaxation and the sub-Rouse modes, and via the CM Eq. (1) results in the shifts of $\tau_{\alpha}$ and $\tau_{\rm sR}$ to shorter time in the thin film. However, the shift of $\tau_{\alpha}$ is much larger than $\tau_{\rm sR}$ and this explains the apparent reduction of the plateau compliance in the experimental measurement of compliance.[100,101] The effects become larger on decreasing film thickness $h$, and in polymer with larger $n_{\alpha}$. These predictions were verified by experiments performed on polymers with different values of $n_{\alpha}$.[101]

Another application of the CM made on polymer chain dynamics found by simulations and dielectric experiment performed on binary polymer blends with the two components having large difference in mobility (or $T_{\rm g}$).[102] The molecular weights $M$ of both are below the entanglement molecular weight $M_{\rm c}$, and hence the chains are not entangled. Before blending the two components together, the chains dynamics obey the Rouse model, with $\exp(-t/\tau_{\rm R})$ for the correlation function and $\tau_{\rm R}$ having the $M^2$-dependence. However in the blend, the chain normal mode of the fast component has its correlation function changed to $\exp[-(t/\tau)^{1-n}]$, with $\tau$ having the $M^{2/(1-n)}$-dependence. This interesting $M^{2/(1-n)}$-dependence follows from the CM Eq. (1) after taking into consideration of the $M^2$-dependence of the primitive relaxation time $\tau_{\rm R}$ appearing on the right-hand-side.[34] Also observed is $(1-n)$ decreasing on decreasing $T$. This trend is due to increasing disparity in mobility of the two components at lower temperatures, which causes increasing constraint imposed on the chains of the faster component by the slower component, and larger chain coupling parameter $n$. At the lowest $T$ studied, $2/(1-n) \approx 3.6$, and $\tau \propto M^{3.6}$. These results are examples of universal properties manifested in the dynamics of polymer chains, which also is consistent with the CM Eq. (1) when applied to this case.[27] The $M^{2/(1-n)}$-dependence of the relaxation time of the unentangled chains in polymer blends resembles the $M^{3.4}$-dependence of the terminal relaxation time of entangled polymer chain in high molecular weight polymer. The latter also had been explained by the CM together with the temperature dependence.[11,76,81,87] This analogy is unsurprising because determined by inter-chain interaction, entangled polymer dynamics is just another case of many-body relaxation of interacting system.

## 5. Breakdown of Stokes–Einstein relation and related phenomena

Measurements of dynamics in glass-forming liquids indicate that the shear viscosity $\eta$, the rotational correlation time $\tau_{\rm c}$, and the self-diffusion coefficient $D$ all slow down dramatically with decreasing temperature.[103–109] However, the products $D\eta$ and $D\tau_{\rm c}$ are not constant but increase as the temperature is lowered toward $T_{\rm g}$ as seen in 1,3-bis-(1-naphthyl)-5-(2-naphthyl)benzene (TNB), OTP, IMC, and other glass-formers. Hence the Stokes–Einstein (SE) and the Debye–Stokes–Einstein (DSE) relations are no longer valid. One explanation offered is based upon the spatially heterogeneous dynamics in supercooled liquids.[103–106] The regions of differing dynamics give rise to the Kohlrausch relaxation function in ensemble averaging measurements. The decoupling between self-diffusion and rotation occurs because $D$ and $\tau_{\rm c}$ are averages over different moments of the distribution of relaxation time, with $D \propto \langle 1/\tau \rangle$ emphasizing fast dynamics, while $\tau_{\rm c} \propto \langle \tau \rangle$ is determined predominantly by the slowest molecules. In order for this explanation to be consistent with the observed monotonic increases of the products $D\eta$ and $D\tau_{\rm c}$ as the temperature is lowered toward $T_{\rm g}$, the breadth of the relaxation time distribution has to increase (or the Kohlrausch exponent, $1-n$, has to decrease) correspondingly. However, Richert and coworkers[110,111] have recently reported that the dielectric spectra of TNB and OTP have a temperature independent width (e.g., $1-n_{\rm d}$ is constant equal to 0.50) from 345 K to 417 K in the case of TNB. The $T_{\rm g}$ of TNB is 342 K. Photon correlation spectroscopic[112] and NMR[113] measurements all indicate a temperature-independent distribution of relaxation time up to about 10% above $T_{\rm g}$. Thus, these data of TNB as well as similar results found in o-terphenyl and sucrose benzoate[114] have invalidated the popular explanation that was believed true for more than 2 decades. In a recent review on supercooled liquids and glasses,[98] the authors have made clear that this explanation contradicts experiments and simulations, and is defunct. Does this situation mean that now there is no explanation of the breakdown of SE and DSE relations? The answer is no. Actually an alternative explanation was given in 1999 by the coupling model,[115,116] which has been eclipsed by the spatially heterogeneous dynamics explanation and is still not mentioned in the review[98] after conceding that the latter is inconsistent with experiments. Possi-

bly this is due to a misunderstanding or mistake made in another review[117] that relaxation in the CM is a homogeneous process. Although it was made amply clear in the 1999 CM papers[105,106] that relaxation is dynamically heterogeneous.

In the explanation given by the CM,[115,116] it is pointed out that the breakdown of the SE and DSE relations in glass-forming liquids is special cases of a more general phenomenon in many-body relaxation and diffusion that different dynamic observables $\mu$ weigh the slowing down in many-body relaxation differently. In the CM, this corresponds to different $\mu$ having different coupling parameters $n_\mu$ (i.e., degrees of intermolecular cooperativity), which enter into the stretch exponents of their correlation functions,[115,116,118–120]

$$\langle\mu(0)\mu(t)\rangle/\langle\mu^2(0)\rangle = \exp[-(t/\tau_\mu)^{1-n_\mu}]. \quad (5)$$

Applying Eqs. (1) and (2) or (3) to each observable $\mu$, we can immediately see that the observable having a larger $n_\mu$ will bestow a stronger temperature dependence for its relaxation time $\tau_{\alpha\mu}$, This is because in the CM, the primitive relaxation time of all the observables, $\tau_{0\mu}$, uninfluenced by many-body relaxation dynamics, should have one and the same temperature dependence. Although the value of $n_\eta$ for viscosity is known from fits to shear compliance measurement[107,108] or light scattering data ($n = 0.45$),[112] $n_{\rm d}$ for dielectric relaxation[110,111] and NMR[113] is 0.50, $n_{\rm D}$ for self diffusion is not yet available from experiment. Nevertheless, theoretical arguments have been given before to show that $n_\eta$ is larger than $n_{\rm D}$,[115] and the explanation of the breakdown of the SE and DSE relations follows from the CM by this relation.

This CM explanation holds independent of whether $n_{\rm d}$ and $n_\eta$ are temperature dependent or independent. We demonstrate this for TNB by taking $n_{\rm d} = 0.50$ of shear creep compliance (and viscosity $\eta$) or dielectric relaxation to be temperature independent from below $T_{\rm g} = 342$ K to 417 K as found for dielectric relaxation by Richert *et al*. The recoverable shear creep compliance, $J_{\rm r}(t)$, data near and above $T_{\rm g}$ of TNB in Refs. [107] and [108] have been fitted by the function

$$J_{\rm r}(t) = J_{\rm g} + (J_{\rm e} - J_{\rm g})\{1 - \exp[-(t/\tau_{\alpha\eta})^{1-n_\eta}]\}, \quad (6)$$

where $J_{\rm g}$ and $J_{\rm e}$ are the glassy and the steady state compliances, respectively, and $n_\eta$ is also close to 0.50. In Fig. 18, the data of $T/\eta(T)$ have been shifted by a constant so that the value is $10^3$ s at $T_{\rm g}$ of TNB, and represent the shear compliance retardation time $\tau_{\alpha\eta}(T)$. The self-diffusion constant $D(T)$ data from three sources[104,107,121] are also shifted by a constant to overlap with the shifted data of $T/\eta(T)$ at high temperatures,[108,109] and represent the self-diffusion time $\tau_{\alpha{\rm D}}(T)$. These operations are similar to the other ways done by others[106] reproduced in the inset.

With these values of $\tau_{\alpha\eta}(T)$ and $t_{\rm c}$ known to be equal to about 2 ps, equation (1) is used to calculate the primitive relaxation time $\tau_{0\eta}(T)$. We assume that the primitive self-diffusion relaxation time $\tau_{0{\rm D}}$ is the same as $\tau_{0\eta}$, and calculate $\tau_{\alpha{\rm D}}(T)$ by using a $n_{\rm D}$ to have a smaller value than $n_\eta = 0.50$ as suggested by the CM explanation.[115] In Fig. 18, we present the results of $\tau_{0\eta}(T)$ calculated with the temperature independent $n_\eta = 0.50$. Based on $\tau_{0\eta}$ and assuming $\tau_{0{\rm D}} = \tau_{0\eta}$, the values of $\tau_{\alpha{\rm D}}(T)$ are calculated by Eq. (1) now with constant $n_{\rm D} = 0.40$ and again $t_{\rm c} = 2$ ps. The calculated $\tau_{\alpha{\rm D}}(T)$ are in good agreement with the experimental values, and the CM can successfully explain the breakdown of the SE relation in the case when $n_\eta$ or $n_{\rm d}$ is constant and independent of temperature.[110–114] The CM explanation remains valid in view of the finding of the temperature-independent distribution of relaxation time as found in TNB, OTP, and IMC.

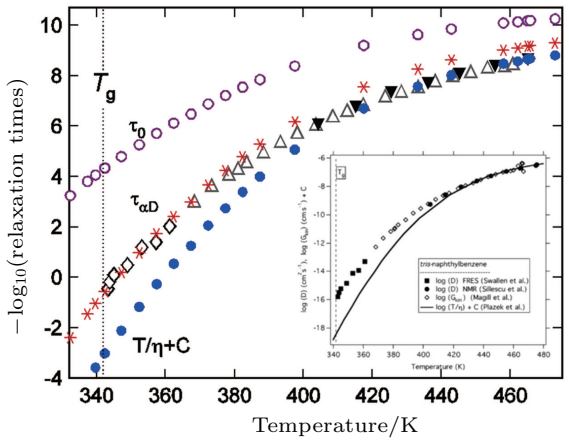



**Fig. 18.** (color online) The CM explanation of the breakdown of the SE relation of TNB by comparing the temperature dependence of $\tau_{\alpha{\rm D}}(T)$ with that of $T/\eta$. For details see text. The shear viscosity data are taken from the works of Plazek and Magill.[108] For comparison, the actual values of $T/\eta$ have been shifted vertically (shown by closed circles) to represent $\tau_{\alpha\eta}(T)$ and such that its value at $T_{\rm g}$ is about $10^3$ s. The inset is taken from Ref. [106] and reproduced by permission.

### 5.1. Support of the CM explanation from molecular dynamics simulations

Chakrabarti and Bagchi (CB)[122] performed molecular dynamics simulation of an equimolar mixture of Gay–Berne ellipsoids of revolution and Lennard–Jones spheres along an isochore at a series of temperatures down to the deeply supercooled state. For this system with orientational degrees of freedom, CB obtained for the ellipsoids of revolution the self intermediate scattering function $F_{\rm s}(k_{\rm max},t)$, and the first and the second rank single particle orientational time correlation functions, $C_1(t)$ and $C_2(t)$, involving respectively the first order and the second order Legendre polynomials. All three functions have time dependences well described by the Kohlrausch functions at all temperatures. The Kohlrausch correlation time and exponent are designated by $\tau_{\rm D}(T)$ and $\beta_{\rm D}(T) \equiv (1 - n_{\rm D}(T))$ for $F_{\rm s}(k_{\rm max},\ t)$; $\tau_1(T)$ and $\beta_1(T) \equiv (1 - n_1(T))$ for $C_1(t)$;

and $\tau_2(T)$ and $\beta_2(T) \equiv (1-n_2(T))$ for $C_2(t)$. The values of $n_{\rm D}(T)$, $n_1(T)$, and $n_2(T)$ are reproduced in Fig. 19. It can be seen from the figure that all of them are very close to zero at high temperatures and increase as temperature falls. At high temperatures, $0.7 < T \leq 2.0$, $n_{\rm D}(T)$ and $n_2(T)$ are both smaller and nearly the same, and the product $D(T)\tau_2(T)$ is nearly independent of temperature as predicted by the DSE relation. However, as temperature is falling below $T = 0.7$, $n_{\rm D}(T)$ and $n_2(T)$ increase rapidly and $n_{\rm D}(T)$ becomes increasingly less than $n_2(T)$. Simultaneously, the product $D(T)\tau_2(T)$ increases rapidly from its nearly constant value at high temperature by a factor of about 2 from $T = 0.7$ down to $T = 0.5$ (see Fig. 3 of CB), i.e., $[D\tau_2(T=0.5)/(D\tau_2)_{{\rm high}T}] \approx 2$. It is helpful to point out here in the CM (Eq. (4)) that the ratio $\tau_2(T)/\tau_{\rm D}(T)$ or the product $D(T)\tau_2(T)$ depends not only on the difference $n_2(T) - n_{\rm D}(T)$, but also on the magnitude of $n_2(T)$ or $n_{\rm D}(T)$. Even for the same $n_2(T) - n_{\rm D}(T)$, $D(T)\tau_2(T)$ increases with increasing $n_2(T)$ or $n_{\rm D}(T)$, and explains the data of CB. Therefore, the molecular dynamics simulation data of CB verify that the breakdown of the DSE relation is associated with $n_{\rm D}(T)$ becoming smaller than $n_2(T)$, and support the CM explanation.[116]

Compared with $D(T)\tau_2(T)$, $D(T)\tau_1(T)$ shows much weaker temperature dependence. This observed behavior of $D(T)\tau_1(T)$ with temperature poses difficulty to the explanation for the decoupling between rotational and translational diffusions in terms of dynamical heterogeneity.[103–106] Moreover, rough estimates of data in Figs. 2(a) and (3) of CB give $[D\tau_1(T=0.5)/(D\tau_1)_{{\rm high}T}] \approx 0.7$, which indicates the breakdown of the SE and DSE relations exhibited by $D(T)\tau_1(T)$ in opposite direction of $D(T)\tau_2(T)$. However, these behaviors of $D(T)\tau_1(T)$ are consistent with the CM because $n_1(T) < n_D(T)$ (see Fig. 19).

CB found that the ratio $\tau_1(T)/\tau_2(T)$ has a value close to 3 at high temperatures when both $n_1(T)$ and $n_2(T)$ are small as expected for the ratio of the first to second rank rotational correlation time of the Debye model involving small steps in orientational motion. The ratio starts to decrease monotonically at $T \approx 1.0$ until it reaches a value nearly unity at low temperatures of $T \approx 0.5$. Values of $\tau_1(T)/\tau_2(T)$ larger than 3 were observed in molecular dynamics simulations of a model polymer.[123] The deviation is in opposite direction to that found by CB in their system, but interestingly the $n_1(T)$ is larger than $n_2(T)$. For example, in one polymer chain of length 500 at 300 K, $\beta_1 \equiv (1-n_1) = 0.399$ and $\tau_1 = 94.7$ ps, while $\beta_2 \equiv (1-n_2) = 0.498$ and $\tau_2 = 9.79$ ps. The result that $\tau_1/\tau_2$ is more than three times larger than 3 is explained by the CM by the fact that $n_1(T)$ is larger than $n_2(T)$.[119] The CM can also explain the result when $\tau_1/\tau_2$ is less than 3 in the system simulated by CB because here $n_1$ is smaller than $n_2$ at lower temperatures. The CM predicts for two observables $\mu_1$ and $\mu_2$, if $n_{\gamma 1}$ is larger than $n_{\gamma 2}$ then the temperature dependence of the relaxation time of $\mu_1$ will be stronger than that of $\mu_1$. Experimental data that support this prediction are given in Refs. [115], [116], and [120].

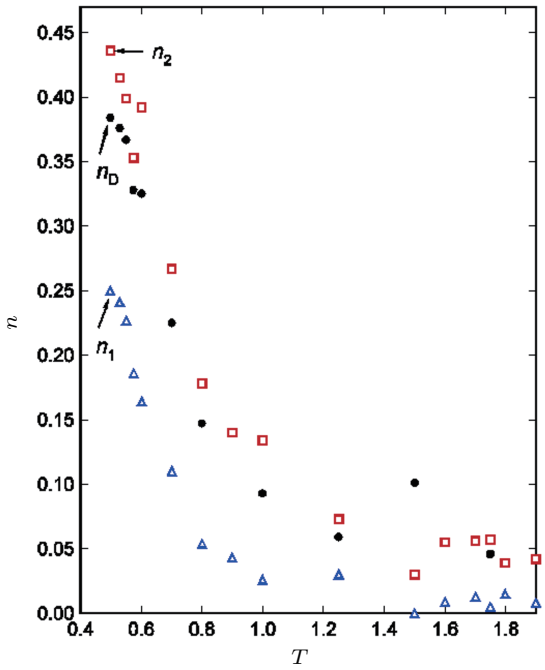



**Fig. 19.** (color online) The values of $n_{\rm D}(T)$, $n_1(T)$, and $n_2(T)$ obtained from the simulation results of Chakarbarty and Bagchi Ref. [122] replotted as a function of temperature.

### 5.2. Limit of applicability of dynamic heterogeneity to explain other properties

In a perspective on supercooled liquids and glasses, the authors[98] stressed that spatially heterogeneous dynamics, or dynamic heterogeneity, is a general feature of supercooled liquids. This is an inarguable fact supported by experimental evidences and computer simulations. However, it fails to explain another property of supercooled liquids, namely, the breakdown of the SE and DSE relations. The failure is because dynamic heterogeneity is one of the several notable parallel consequences of the many-body relaxation, and it is unsurprising that one consequence may not be able to explain another one.

Another example of the limit of applicability of dynamic heterogeneity is the failure to explain thermo-rheological complexity of polymers. Such attempt was made by the authors of Ref. [97], who indeed ascribed the different temperature-dependences of the segmental and chain motions (a property observed in many polymers[123]) to the effect of dynamic heterogeneities on the former being averaged out over the longer length and time scales of the latter. This was reiterated by the authors of the perspective[98] in making the statement: "In polymer melts, spatially heterogeneous dynamics leads to the failure of the 'single time scale' picture in an additional manner, with the temperature dependence of segmental and large scale chain motions being dissimilar for fragile systems.[155]"

Reference [155] cited in this statement is Ref. [97] here. However, as pointed out as a comment[124] on Ref. [97], this explanation does not account for the related decoupling of the self-diffusion constant and viscosity of entangled polymers. Furthermore, the apparent activation energy for self-diffusion in some polymers with low $T_g$ is significantly smaller than for the viscosity,[76] similar to the difference in temperature dependence of the segmental and chain dynamics. The self-diffusion constant and the viscosity of entangled polymers both involve global motions; i.e., they entail length scales large compared to the dynamic heterogeneities. Thus, spatially heterogeneous dynamics cannot be the primary origin of the differences in temperature dependences for polymers. Distinct averaging over the length and time scales cannot underlie differences between properties that both involve chain relaxation.

### 5.3. Support of the CM explanation from ionic conductors

Ion conductivity relaxation data measured by electrical conductivity relaxation (ECR) experiment can be compared with ion diffusion data measured by nuclear spin-lattice relaxation (SLR). Combined studies of ion dynamics using ECR and SLR were first reported at almost the same time by Tatsumisago *et al.* in Li chloroborate glasses[125,126] and by Kanert and coworkers in heavy metal flurozirconate glasses,[127–129] and found large difference between the ECR and SLR results. At some temperatures, the NSR correlation time of the mobile ion, $\tau_s$, is several orders of magnitude longer than the ECR time, $\tau_\sigma$, while the thermal activation energy of $\tau_s$, $E_s$, is significantly larger than $E_\sigma$ of $\tau_\sigma$.

Since the two techniques are monitoring motion of the ions, it is puzzling that there is such a pronounced difference between SLR and ECR in their relaxation times and activation energies. Similar differences were subsequently observed in other superionic glasses including $(Li_2S)_{0.56}(SiS_2)_{0.44}$,[130] $x(Li_2S)+(1-x)GeS_2$,[131] and $x(Li_2S)+(1-x)B_2S_3$,[132] and in crystalline Na$\beta$-$Al_2O_3$,[133] confirming that the effect can be considered as a general property of ionic conductors. The computer experiments by Monte Carlo simulation of ionic motion in disordered lattices, taking into account the Coulomb interactions between the mobile ions,[134] found the same difference between SLR and ECR as in real experiments. The data of $(Li_2S)_{0.56}(SiS_2)_{0.44}$ are shown in Fig. 20.

The longer $\tau_s$ than $\tau_\sigma$ and larger $E_s$ than $E_\sigma$ found in ionic conductors are rightfully the analogues of the breakdown of SE and DSE relations in supercooled liquids, but there is no dynamic heterogeneity in these glassy ionic conductors to speak about and use to explain the differences. The explanation comes from the CM described as follows.

It is found in experiments that both the ECR and NSR correlation functions depart from a pure exponential behavior and have the Kohlrausch forms and Arrhenius $T$-dependences for their relaxation times

$$\phi_\sigma(t) = \exp[-(t/\tau_\sigma)^{1-n_\sigma}], \tag{7}$$

where $\tau_\sigma = \tau_{\sigma,\infty}\exp(E_\sigma/kT)$, and

$$\phi_s(t) = \exp[-(t/\tau_s)^{1-n_s}], \tag{8}$$

where $\tau_s = \tau_{s,\infty}\exp(E_s/kT)$. The parameters $n_\sigma$, $E_\sigma$, $n_s$, and $E_s$ of the ionic conductors are presented in Table 1. As already mentioned, the relations $\tau_s \gg \tau_\sigma$ and $E_s > E_\sigma$ were reported in experimental studies and simulations. Moreover, it was found that $n_s > n_\sigma$.

These differences found experimentally between SLR and ECR have been explained and rationalized within the CM.[135–140] From experiments of the glassy ionic conductors, the relation $n_s > n_\sigma$ leads to the stronger temperature dependence of $\tau_s$ than $\tau_\sigma$ or the relation $E_s > E_\sigma$ is explained by the CM Eq. (1). Moreover, a quantitative test is afforded by comparing the products $(1-n_s)E_s$ with $(1-n_\sigma)E_\sigma$. They should be equal according to the CM, and indeed this is the case (see Table 1).

**Table 1.** The activation energy $E_s$ and coupling parameters $n_s$ for SLR, and the corresponding quantities, $E_\sigma$, and $n_\sigma$ for ECR for three different glassy ionic conductors.

| Ionic conductor | Dynamic variable $U$ | $\beta_U \equiv (1-n_U)$ | $E_U^*/K$ | $(1-n_U)E_U^*/K$ |
|---|---|---|---|---|
| $(Li_2S)_{0.56}(SiS_2)_{0.44}$ | spin (SLR) | 0.35 | 5845 | 2046 |
| $(Li_2S)_{0.56}(SiS_2)_{0.44}$ | $\sigma$ (ECR) | 0.52 | 3911 | 2034 |
| $(Li_2S)_{0.45}(GeS_2)_{0.55}$ | spin (SLR) | 0.34 | 5750 | 1950 |
| $(Li_2S)_{0.45}(GeS_2)_{0.55}$ | $\sigma$ (ECR) | 0.44 | 4730 | 2080 |
| $(LiCl)_{0.6}(Li_2O)_{0.7}(B_2O_3)$ | spin (SLR) | 0.35 | 7400 | 2590 |
| $(LiCl)_{0.6}(Li_2O)_{0.7}(B_2O_3)$ | $\sigma$ (ECR) | 0.50 | 5500 | 2750 |
| ZBLAN[a)] | spin (SLR) | 0.30 | 13346 | 3830 |
| ZBLAN[a)] | $\sigma$ (ECR) | 0.44 | 9284 | 4085 |

[a)] 27.4 ZrF, 27.4 HfF, 19.8 BaF, 3 LaF, 3.2 $A1F_3$, 20 NaF (in mol%)

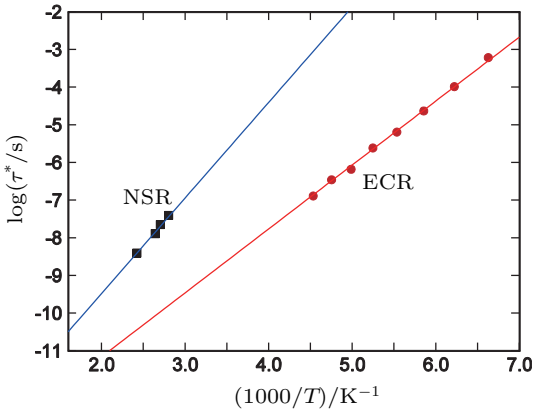



**Fig. 20.** (color online) Arrhenius plots of the correlation time $\tau_s$ deduced from $^7$Li NMR spin-lattice relaxation measurement and $\tau_M$ from electrical conductivity measurement for $(Li_2S)_{0.56}(SiS_2)_{0.44}$.

## 6. Conclusion and perspectives

The main purpose of writing this review is to let more researchers in condensed matter physics and chemistry as wells as in materials sciences to be aware of the existence of universal properties in relaxation and diffusion in substances, materials, and systems of diverse physical and chemical structures. The examples chosen in this review are sufficient to support the universality. There are many more but they cannot be mentioned here in order to make the size of this review reasonable. There is no doubt that the universality has been firmly established by experiments and simulations, and it should be recognized as an important discovery.

The universal properties originate from the many-body nature of the irreversible processes in interacting systems, which are governed by some fundamental physics likely related to classical chaos because of the potential of interaction is usually anharmonic. Recognition of the universality not only benefits progress of research in many different fields, but also makes clear that it is an important and unsolved problem in statistical mechanics of complex interacting systems. Although neither it is a rigorous nor complete solution of relaxation and diffusion of many-body interacting systems, the coupling model has been proven successful to explain many of the universal properties, and to solve problems in various disciplines. It can be used as a stepping stone for others in constructing a rigorous and fundamental theory to solve the fundamental problem once and for all.

## Acknowledgment

I thank all my collaborators in the papers cited in this review for their contributions, and Prof. Li-Min Wang, Prof. H. Y. Bai, and Prof. W. H. Wang for collaboration and hospitality during my annual visit to their laboratories in China for the past six years.

## References

[1] Einstein A 1905 *Ann. D. Physik* **17** 549
[2] Brown R 1828 *Philos. Mag.* **4** 161
[3] Lichtenberg A L and Lieberman M A 1992 *Regular and Chaotic Dynamics* (New York: Springer)
[4] Berry M V 1987 *Proc. R. Soc. Lond. A* **413** 183
[5] Gutzwiller M C 1990 *Chaos in Classical and Quantum Mechanics* (New York: Springer)
[6] Ngai K L 1979 *Comment Solid State Phys.* **9** 127
[7] Tsang K Y and Ngai K L 1996 *Phys. Rev. E* **54** R3067
[8] Tsang K Y and Ngai K L 1997 *Phys. Rev. E* **56** R17
[9] Rendell R W 1993 *Phys. Rev. E* **48** R17
[10] Ngai K L and Tsang K Y 1999 *Phys. Rev. E* **60** 4511
[11] Ngai K L 2011 *Relaxation and Diffusion in Complex System* (New York: Springer)
[12] Habasaki J, Leon C and Ngai K L 2016 *Dynamics of Glassy, Crystalline, and Liquid Ionic Conductors* (New York: Springer)
[13] Bedrov D and Smith G D 2011 *J. Non-Cryst. Solids* **357** 258
[14] Mattsson J, Wyss H M, Fernandez-Nieves A, Miyazaki K, Hu Z, Reichman D R and Weitz D A 2009 *Nature* **462** 83
[15] Kessairi K, Capaccioli S, Prevosto D, Lucchesi M, Sharifi S and Rolla P A 2008 *J. Phys. Chem. B* **112** 4470
[16] Ferry J D 1980 *Viscoelastic Properties of Polymers*, 3rd ed., (New York:Wiley)
[17] Adam G and Gibbs J H 1965 *J. Chem. Phys.* **43** 139
[18] Götze W 1999 *J. Phys.: Condens. Matter* **11** A1
[19] Götze W 2009 *Complex Dynamics of Glass-Forming Liquids*, International Series of Monographs on Physics 143, Oxford Science Publications, Oxford (2009)
[20] Stevenson J D and Wolynes P G 2011 *J. Phys. Chem. A* **115** 3713
[21] Ngai K L, Casalini R, Capaccioli S, Paluch M and Roland C M 2005 *J. Phys. Chem. B* **109** 17356
[22] Mierzwa M, Pawlus S, Paluch M, Kaminska E and Ngai K L 2008 *J. Chem. Phys.* **128** 044512
[23] Capaccioli S, Paluch M, Prevosto D, Wang L M and Ngai K L 2012 *J. Phys. Chem. Lett.* **3** 735
[24] Jarosz G, Mierzwa M, Ziolo J, Paluch M, Shirota H and Ngai K L 2011 *J. Phys. Chem. B* **115** 12709
[25] Roland C M, Hensel-Bielowka S, Paluch M and Casalini R 2005 *Rep. Prog. Phys.* **68** 1405
[26] Floudas G, Paluch M, Grzybowski A and Ngai K L 2011 *Molecular Dynamics of Glass-Forming Systems: Effects of Pressure* (Berlin: Springer-Verlag)
[27] Ngai K L 1998 *J. Chem. Phys.* **109** 6982
[28] Ngai K L and Paluch M 2004 *J. Chem. Phys.* **120** 857
[29] Johari G P, Goldstein M 1970 *J. Chem. Phys.* **53** 2372
[30] Johari G P 1976 *Ann. N Y Acad. Sci.* **279** 117
[31] Ngai K L 2003 *J. Phys.: Condens. Matter* **15** S1107
[32] Brand R, Lunkenheimer P and Loidl A 2002 *J. Chem. Phys.* **116** 10386
[33] Romanini M, Negrier Ph, Ll. Tamarit J, Capaccioli S, Barrio M, Pardo L C and Mondieig D 2012 *Phys. Rev. B* **85** 134201
[34] Ngai K L and Capaccioli S 2013 *J. Chem. Phys.* **138** 054903
[35] Yu H B, Wang W H, Bai H Y and Samwer K 2014 *National Science Review* **1** 429
[36] Yu H B, Shen X and Wang Z 2012 *Phys. Rev. Lett.* **108** 015504
[37] Qiao J and Pelletier J M 2012 *J. Appl. Phys.* **112** 083528
[38] Zhu Z G, Li Y Z, Wang Z, Gao X Q, Wen P, Bai H Y, Ngai K L and Wang W H 2014 *J. Chem. Phys.* **141** 084506
[39] Brás A R, Noronha J P, Antunes A M M, Cardoso M M, Schönhals A, Affouard F, Dionísio M and Correia N T 2008 *J. Phys. Chem. B* **112** 11087
[40] Kaminski K, Kaminska E, Wlodarczyk P, Pawlus S, Kimla D, Kasprzycka A, Paluch M, Ziolo J, SzejaWand Ngai K L 2006 *J. Phys. Chem. B* **110** 25045
[41] Kaminski K, Kaminska E, Wlodarczyk P, Pawlus S, Kimla D, Kasprzycka A, Paluch M, Ziolo J, SzejaW and Ngai K L 2008 *J. Phys. Chem. B* **112** 12816
[42] Capaccioli S, Ngai K L and Shinyashiki N 2007 *J. Phys. Chem. B* **111** 8197
[43] Ngai K L, Capaccioli S, Ancherbak S and Shinyashiki N 2011 *Philos. Mag.* **91** 1809
[44] Shinyashiki N, Yamamoto W, Yokohama A, Toshihari T, Yagihara S, Kita R, Ngai K L and Capaccioli S 2009 *J. Phys. Chem. B* **113** 14448
[45] Ngai K L, Capaccioli S and Paciaroni A 2013 *Chem. Phys.* **424** 37

[46] Ngai K L, Capaccioli S and Paciaroni A 2016 *Biochim. Biophys. Acta*
[47] Ngai K L, Habasaki J, Prevosto D, Capaccioli D and Paluch M 2012 *J. Chem. Phys.* **137** 034511
[48] Coslovich D and Roland C M 2008 *J. Phys. Chem. B* **112** 1329
[49] Anastasiadis S H, Karatasos K, Vlachos G, Manias E and Giannelis E P 2000 *Phys. Rev. Lett.* **84** 915
[50] Ngai K L 2002 *Philos. Mag.* **82** 291
[51] Ngai K L 2002 *Eur. Phys. J. E* **8** 225
[52] Ngai K L 2006 *J. Polym. Sci. B: Polym. Phys.* **44** 2980
[53] Patkowski A, Ruths T and Fischer E W 2003 *Phys. Rev. E* **67** 021501
[54] Ngai K L 1999 *J. Phys.: Condens. Matter* **11** A119
[55] Schönhals A, Goering H, Schick Ch, Frick B and Zorn R 2004 *Colloid Polym. Sci.* **282** 882
[56] Schönhals A, Goering H, Schick Ch, Frick B and Zorn R 2005 *J. Non-Cryst.Solids* **351** 2668
[57] Beiner M and Huth H 2003 *Nat. Mater.* **2** 595
[58] Ngai K L and Beiner M 2004 *Macromolecules* **37** 8123
[59] Beiner M 2006 *AIP Conf. Proc.* **832** 134
[60] Zhu L, Brian C W, Swallen S F, Straus P T, Ediger M D and Yu L 2011 *Phys. Rev. Lett.* **106** 256103
[61] Capaccioli S, Ngai K L, Paluch M and Prevosto D 2012 *Phys. Rev. E* **86** 051503
[62] Zhang W, Brian C W and Yu L 2015 *J. Phys. Chem. B* **119** 5071
[63] Cao C R, Lu Y M, Bai H Y and Wang H W 2015 *Appl. Phys. Lett.* **107** 141606
[64] Teichler H 1996 *Phys. Rev. Lett.* **76** 62
[65] Han X J and Schober H R 2011 *Phys. Rev. B* **83** 224201
[66] Ngai K L, Capaccioli S, Cao C R, Bai H Y and Wang H W, to be published.
[67] Bokeloh J, Divinski S V, Reglitz G and Wilde G 2011 *Phys. Rev. Lett.* **107** 235503
[68] Ngai K L and Yu H B 2013 *J. Appl. Phys.* **113** 103508
[69] Ngai K L, Santamaria J and Leon C 2013 *Euro. Phys. J. B* **86** 7
[70] Kosacki I, Rouleau C M, Becher P F, Bentley J and Lowndes D H 2005 *Solid State Ionics* **176** 1319
[71] Plazek D J and O'Rourke V M 1971 *J. Polym. Sci. A* **9** 209
[72] Gray R W, Harrison G and Lamb J 1977 *Proc. R. Soc. London A* **356** 77
[73] Plazek D J 1980 *Polymer J.* **12** 43
[74] Plazek D J 1996 *J. Rheology* **40** 987
[75] Ngai K L and Plazek D J 1995 *Rubber Chem. Technol. Rubber Rev.* **68** 376
[76] McKenna G B, Ngai K L and Plazek D J 1985 *Polymer* **26** 1651
[77] Plazek D L and Plazek D J 1983 *Macromolecules* **16** 1469
[78] Ngai K L and Fytas G 1986 *J. Polym. Sci. B: Polym. Phys.* **24** 1683
[79] Floudas G, Gravalides C, Reisinger T G and Wegner J 1999 *Chem. Phys.* **111** 9847
[80] Floudas G 2004 *Prog. Polym. Sci.* **29** 1143
[81] Ngai K L and Plazek D J 1986 *J. Polym. Sci. B: Polym. Phys.* **24** 619
[82] Ngai K L, Plazek D J and Deo S S 1987 *Macromolecules* **20** 3047
[83] Plazek D J, Bero C, Neumeister S, Floudas G, Fytas G and Ngai K L 1994 *J. Colloid Polymer Sci.* **272** 1430
[84] Plazek D J, Schönhals A, Schlosser E and Ngai K L 1993 *J. Chem. Phys.* **98** 6488
[85] Plazek D J, Chay I C, Ngai K L, Roland C M 1995 *Macromolecules* **28** 6432
[86] Ngai K L, Plazek D J and Rizos A K 1997 *J. Polymer Sci. B: Polym. Phys.* **35** 599
[87] Ngai K L, Plazek D J and Rendell R W 1997 *Rheol. Acta* **36** 307
[88] Roland C M, Ngai K L and Plazek D J 2004 *Macromolecules* **37** 7051
[89] Ngai K L and Plazek D J 2002 *Macromolecules* **35** 9136
[90] Ngai K L, Casalini R and Roland C M 2005 *Macromolecules* **38** 4363
[91] Wu X B, Liu C S, Zhu Z G, Ngai K L and Wang L M 2011 *Macromolecules* **44** 3605
[92] Wu X B and Zhu Z G 2009 *J. Phys. Chem. B* **113** 11147
[93] Wu J, Huang G, Wang X, He X and Xu B 2012 *Macromolecules* **45** 8051
[94] Ngai K L and Plazek D J 2014 *Macromolecules* **47** 8056
[95] Wu X B, Liu C S and Ngai K L 2014 *Soft Matter* **10** 9324
[96] Ngai K L, Prevosto D and Grassia L 2013 *J. Polym. Sci. B: Polym. Phys.* **51** 214
[97] Sokolov A P and Schweizer K S 2009 *Phys. Rev. Lett.* **102** 248301
[98] Ediger M D and Harrowell P 2012 *J. Chem. Phys.* **137** 080901
[99] Ngai K L and Roland C M 2013 *J. Chem. Phys.* **139** 036101
[100] O'Connell P A, Hutcheson S A and McKenna G B 2008 *J. Polym. Sci. B: Polym. Phys.* **46** 1952
[101] Li X and McKenna G B 2015 *Macromolecules* **48** 6329
[102] Arrese-Igor S, Alegria A, Moreno A J and Colmenero J 2012 *Soft Matter* **8** 3739
[103] Cicerone M T, Blackburn F R and Ediger M D 1995 *J. Chem. Phys.* **102** 471
[104] Chang I and Sillescu H 1997 *J. Phys. Chem. B* **101** 8794
[105] Hooker J C and Torkelson J M 1995 *Macromolecules* **28** 7683
[106] Mapes M K, Swallen S F and Ediger M D 2006 *J. Phys. Chem. B* **110** 507
[107] Magill J H and Plazek D J 1967 *J. Chem. Phys.* **46** 3757
[108] Plazek D J and Magill J H 1968 *J. Chem. Phys.* **49** 3678
[109] Ngai K L, Magill J H and Plazek D J 2000 *J. Chem. Phys.* **112** 1887
[110] Richert R, Duvvuri K and Duong L J 2003 *J. Chem. Phys.* **118** 1828
[111] Richert R 2005 *J. Chem. Phys.* **123** 154502
[112] Zhu X R and Wang C H 1986 *J. Chem. Phys.* **84** 6086
[113] Zemke K, Schmidt-Rohr K, Magill J H, Sillescu H and Spiess H W 1993 *Mol. Phys.* **80** 1317
[114] Rajian J R, Huang W, Richert R and Quitevis E L 2006 *J. Chem. Phys.* **124** 014510
[115] Ngai K L 1999 *J. Phys. Chem. B* **103** 10684
[116] Ngai K L 1999 *Philos. Mag. B* **79** 1783
[117] Ediger M D 2000 *Annu. Rev. Phys. Chem.* **51** 99
[118] Ngai K L 2001 *IEEE Trans. Dielect. Electrl Insul.* **8** 329
[119] Ngai K L 1993 *J. Chem. Phys.* **98** 7588
[120] Ngai K L, Mashimo S and Fytas G 1988 *Macromolecules* **21** 3030
[121] Swallen S F, Bonvallet P A, McMahon R J and Ediger M D 2003 *Phys. Rev. Lett.* **90** 015901
[122] Chakrabarti D and B. Bagchi 2006 *Phys. Rev. Lett.* **96** 187801
[123] Takeuchi H and Roe R J 1991 *J. Chem. Phys.* **94** 7446
[124] Ngai K L, Plazek D J and Roland C M 2009 *Phys. Rev. Lett.* **103** 159801
[125] Tatsumisago M, Angell C A and Martin S W 1992 *J. Chem. Phys.* **97** 6968
[126] Angell C A 1992 *Annu. Rev. Phys. Chem.* **43** 693
[127] Estalji S, Kanert O, Steinert J, Jain H and Ngai K L 1991 *Phys. Rev. B* **43** 7481
[128] Estalji S, Küchler R, Kanert O, Bölter R, Jain H and Ngai K L 1992 *Le J. Phys. IV* **02** C2-159
[129] Kanert O, Küchler R, Ngai K L and Jain H 1994 *Phys. Rev. B* **49** 76
[130] Borsa F, Torgeson D R, Martin S W and Patel H K 1992 *Phys. Rev. B* **46** 795
[131] Kim K, Torgeson D R, Borsa F, Cho J, Martin S and Svare I 1996 *Solid State Ionics* **91** 7
[132] Kim K, Torgeson D R, Borsa and Martin S W 1996 *Solid State Ionics* **90** 29
[133] Villa M and Bjorkstam J L 1980 *Phys. Rev. B* **22** 5033
[134] Meyer M, Maass P and Bunde A 1993 *Phys. Rev. Lett.* **71** 573
[135] Ngai K L and Kanert O 1992 *Solid State Ionics* **53–56** 936
[136] Ngai K L 1993 *Solid State Ionics* **61** 345
[137] Ngai K L 1993 *Phys. Rev. B* **48** 13481
[138] Ngai K L 1993 *J. Chem. Phys.* **98** 6424
[139] Ngai K L 1998 *Solid State Ionics* **105** 225
[140] Ngai K L and León C 2003 *J. Non. Cryst. Solids* **315** 124